

CONSTRUCTION AND ACCURACY OF ELECTRONIC CONTINUUM MODELS OF INCOMMENSURATE BILAYER 2D MATERIALS

XUE QUAN, ALEXANDER B. WATSON, AND DANIEL MASSATT

ABSTRACT. Single-particle continuum models such as the popular Bistritzer-MacDonald model have become powerful tools for predicting electronic phenomena of incommensurate 2D materials and developing many-body models aimed at modeling unconventional superconductivity and correlated insulators. In this work, we introduce a procedure to construct continuum models of arbitrary accuracy relative to tight-binding models for moiré incommensurate bilayers. This is done by recognizing the continuum model as arising from Taylor expansions of a high accuracy momentum space approximation of the tight-binding model. We apply our procedure in full detail to two models of twisted bilayer graphene and demonstrate both admit similar Bistritzer-MacDonald models as the leading order continuum model, while higher order expansions reveal qualitative spectral differences.

1. INTRODUCTION

Research on incommensurate stackings of 2D materials has grown rapidly since the discovery of correlated insulator and “unconventional” superconducting states in twisted bilayer graphene (TBG) at the “magic angle” $\approx 1.1^\circ$ in 2018 [10, 11, 19, 34]. To understand these phenomena, which arise from electron-electron correlations, there is a strong push to construct accurate yet tractable many-body models of such materials [6, 18, 28]. Many-body models are generally constructed by the following recipe. First, construct an accurate model for the single-particle electronic properties of the material. Then, extract a basis of energetically relevant states from this model. Finally, project the electron-electron Coulomb interaction to this basis. Hence a careful derivation of an accurate single-particle basis is fundamental.

A key feature of incommensurate stackings of 2D materials at relatively small twist angles is the emergence of approximate periodicity in the atomic structure known as the moiré pattern (see Figure 1.1). The moiré pattern allows for constructing relatively simple single-particle models which are, in particular, periodic with respect to the bilayer moiré pattern. Such models admit a band structure: their spectrum is the union of intervals (bands) swept out by real functions $k \mapsto E_n(k)$, where $n \in \mathbb{Z}$ is known as the band index, and k varies over the moiré Brillouin zone. The associated eigenfunctions of these eigenvalues are Bloch functions $e^{ik \cdot r} u_n(r; k)$, where u_n is moiré-periodic. When constructing many-body models, the energetically relevant single-particle states are usually taken to be the set of Bloch functions associated to the single-particle bands near to the Fermi level.

Date: May 27, 2025.

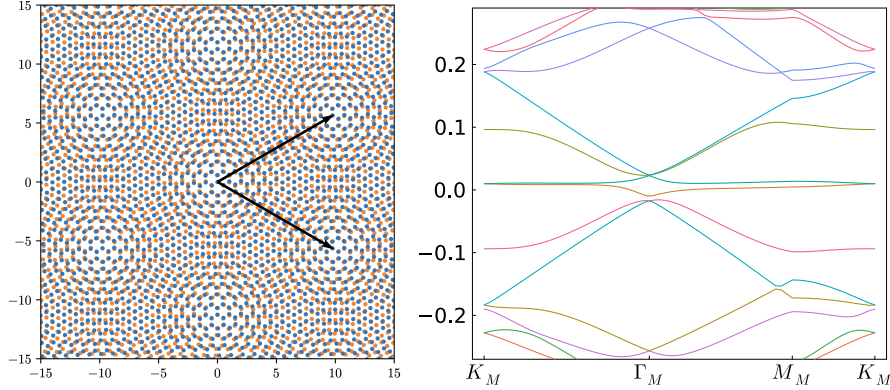


FIGURE 1.1. Left: atomic structure of stacked bilayer graphene with interlayer twist 5° , viewed from above. Atoms in the lower graphene sheet are colored orange and in the upper graphene sheet in blue. Moiré lattice vectors which generate the moiré lattice are shown in black. The continuum models we construct in the present work have coefficients which are periodic with respect to this lattice. Right: band structure of the Bistritzer-MacDonald continuum model [7] at the magic twist angle 1.1° , with parameter values taken from the ab initio tight-binding model proposed in [17]. For more details, see Figure 4.7; this figure is the same as the middle right figure there. Many-body models of twisted bilayer graphene typically model electrons in the flat bands, the two bands nearest to zero energy which are approximately flat over most of the moiré Brillouin zone, interacting via the Coulomb force. Two of the key inputs to such models are the flat band eigenvalues and associated eigenfunctions. The goal of the present work is to construct moiré-scale single-particle continuum models of twisted bilayer graphene's electronic properties with essentially arbitrary accuracy relative to tight-binding models, in order to provide more accurate flat band eigenvalues and eigenfunctions for many-body models.

The most famous moiré-periodic single-particle model for twisted bilayer graphene is the Bistritzer-MacDonald (BM) model [7]. This model comprises a system of continuum Dirac equations, characteristic of the electronic structure of monolayer graphene, coupled through a matrix-valued moiré-periodic potential modeling interlayer hopping depending on the local stacking configuration. This model has been mathematically rigorously justified as an accurate model for electron dynamics under assumptions which are expected to hold in twisted bilayer graphene at the magic angle [32]: specifically, that the twist angle $\theta \ll 1$ (in radians), and that the typical interlayer hopping energy is much less than the typical monolayer hopping energy. For other mathematical derivations, see [8, 9, 27, 35]. The Bistritzer-MacDonald model played an important role in identifying TBG's magic angles, twist angles where the BM model's Bloch bands near to the Fermi level become relatively

flat. This phenomenon is thought to be the reason why magic angle TBG exhibits such a rich many-body phase diagram.

The results of the present work are as follows. First, we introduce a systematic procedure for constructing moiré-periodic single-particle continuum models of TBG in the same regime where the BM model is valid, but to essentially arbitrary accuracy, assuming the validity of an atomic-scale tight-binding model. Second, we rigorously prove convergence of the density of states distribution of the underlying tight-binding model to that of the continuum models we construct. Finally, we compute band structures for the models we construct, comparing the results starting from a simplified tight-binding model as in [32] and a more elaborate model parametrized by density functional theory (DFT) computations [16]. We find that both models admit similar Bistritzer-MacDonald models as their leading-order approximations, but higher-order expansions reveal qualitative differences.

The models we construct account for terms which are neglected in the Bistritzer-MacDonald model, such as higher-order dispersion in the intralayer part of the Hamiltonian, and longer range momentum space hopping and derivative terms in the interlayer part. We emphasize that the energies of these terms are comparable to energy differences between competing many-body ground states in interacting models of twisted bilayer graphene [18], suggesting they may be important in correctly predicting TBG's many-body phase diagram.

The construction works by building on efficient methods for accurately computing the electronic structure of incommensurate two-dimensional multi-layered materials [13, 22–25, 31]. The idea is as follows. First, as in [23, 24], we identify the set of energetically relevant electronic states within each layer; in twisted bilayer graphene these are the states near to the monolayer Dirac points. We then truncate the full tight-binding model to these states, accruing exponentially small error in the truncation threshold as proved in [24]. We then further simplify the truncated model by Taylor-expanding about the Dirac points of each layer. Finally, we realize our accurate models as natural extensions of the truncated model to arbitrary wave-numbers, i.e., taking the continuum limit.

By controlling the error at each step, we obtain error estimates in approximating the density of states distribution in terms of three truncation parameters: the intralayer Taylor-expansion order, interlayer expansion order, and momentum-space hopping distance. In the limit where these parameters become large, we recover the exponential rate of convergence of [24]. These results are summarized in our main result, Theorem 3.1. This approach can be easily generalized to other two-dimensional material stackings such as layered transition metal dichalcogenides and incommensurate trilayer systems, for which moiré-periodic single particle models analogous to the Bistritzer-MacDonald model have been proposed [15, 26].

We finally discuss related mathematical work. In [27], higher-order corrections to the Bistritzer-MacDonald model have been derived following a different methodology from the present work, and proving different results. Specifically, in that work error estimates are proved for the dynamics generated by a tight-binding Schrödinger equation of twisted bilayer graphene by a multiple-scales approach. In [8, 9, 35], moiré-scale continuum models such as the BM model have been derived as approximations of a DFT-informed incommensurate linear Schrödinger model by making use of a semiclassical expansion, with accuracy

quantified for the density of states. In [2–4, 33] insight has been gained into the Bistritzer-MacDonald model’s almost flat bands by studying an approximation of this BM model known as the chiral model introduced in [30]. The chiral model also has an important role in studying TBG’s many-body electronic properties. Many-body models for TBG’s electronic properties have been proposed and solved in [5, 18, 29], although these studies generally rely on the Bistritzer-MacDonald model without the corrections we derive here. Another important aspect of the physics of twisted bilayer graphene near the magic angle are the material’s mechanical/structural properties. The ground state (relaxed) mechanical properties have been investigated in [12, 14, 20], while phonons have been recently considered in [21].

1.1. Structure of paper. The structure of the rest of this paper is as follows. In Section 2, we introduce the momentum space formulation as a transformation of real space tight-binding models and review previous momentum space results we need. In Section 3, we derive continuum models as approximations of momentum space models, and analyze the convergence of the band structure. In Section 4, we verify the convergence results for the simplified TBG and the ab initio Wannierized TBG, and derive high accuracy continuum models for each. The proofs are in the Appendices for clarity of presentation.

1.2. Acknowledgements. ABW’s research was supported in part by NSF grant DMS-2406981. DM’s research was supported in part by AFRL grant FA9550-24-1-0177. XQ’s research was supported by the National Natural Science Foundation of China (No. 12371431).

2. TIGHT-BINDING MODEL

In this work we consider two tight-binding models of twisted bilayer graphene (TBG): the relatively simple model considered in [32], and the more elaborate model proposed in [17] based on ab initio density functional theory calculations. In this section we describe a general tight-binding model of TBG and explain how to obtain the simplified model as a special case of this model.

2.1. Monolayer graphene model. We start by describing a general tight-binding model for an unrotated graphene monolayer. Since graphene is a sheet of carbon atoms arranged in a honeycomb lattice, we introduce Bravais lattice vectors as

$$a_1 := \frac{a}{2}(1, \sqrt{3})^T, \quad a_2 := \frac{a}{2}(-1, \sqrt{3})^T, \quad A := (a_1, a_2),$$

where $a > 0$ is the lattice constant. The graphene Bravais lattice and its unit cell are defined by

$$\mathcal{R} := A\mathbb{Z}^2, \quad \Gamma := A[0, 1)^2.$$

The associated reciprocal lattice and reciprocal lattice unit cell (Brillouin zone) are given by

$$\mathcal{R}^* := 2\pi A^{-T}\mathbb{Z}^2, \quad \Gamma^* := 2\pi A^{-T}[0, 1)^2.$$

The Dirac points, high-symmetry points in the Brillouin zone, play a critical role in the electronic properties of graphene and are given by

$$K := \frac{4\pi}{3a}(1, 0)^T, \quad K' := -K.$$

We further define orbital displacement vectors (with $d := \frac{a}{\sqrt{3}}$):

$$\tau_A := (0, 0)^T, \quad \tau_B := (0, d)^T,$$

so that the two atoms in the R -th lattice are located at $R + \tau_A$ and $R + \tau_B$. Then the real space Hamiltonian can be defined via the infinite matrix

$$H_{R\sigma, R'\sigma'} := h_{\sigma\sigma'}(R - R'),$$

where $h_{\sigma\sigma'} : \mathcal{R} \rightarrow \mathbb{C}$, $h_{\sigma\sigma'} \in \ell^1(\mathcal{R})$. For $\psi = (\psi_R)_{R \in \mathcal{R}} = (\psi_{RA}, \psi_{RB})_{R \in \mathcal{R}}^T \in \ell^2(\mathcal{R} \times \{A, B\})$, H acts as

$$(2.1) \quad (H\psi)_{R\sigma} = \sum_{\sigma' \in \{A, B\}} \sum_{R' \in \mathcal{R}} h_{\sigma\sigma'}(R - R') \psi_{R'\sigma'}.$$

2.2. Twisted bilayer tight-binding model. Twisted bilayer graphene (TBG) consists of two graphene monolayers with a relative twist. We let

$$R(\vartheta) := \begin{pmatrix} \cos \vartheta & -\sin \vartheta \\ \sin \vartheta & \cos \vartheta \end{pmatrix}$$

be the rotation matrix and $\theta > 0$ be the twist angle. The lattice vectors of each layer are defined by

$$a_{1,j} := R\left(-\frac{\theta}{2}\right)a_j, \quad a_{2,j} := R\left(\frac{\theta}{2}\right)a_j, \quad A_j := (a_{j,1}, a_{j,2}).$$

We then have

$$\begin{aligned} \mathcal{R}_j &:= A_j \mathbb{Z}^2, & \Gamma_j &:= A_j [0, 1]^2, \\ \mathcal{R}_j^* &:= 2\pi A_j^{-T} \mathbb{Z}^2, & \Gamma_j^* &:= 2\pi A_j^{-T} [0, 1]^2. \end{aligned}$$

We require the following definition and assumption.

Definition 2.1. *Two Bravais lattices \mathcal{L}_1 and \mathcal{L}_2 are incommensurate if*

$$\mathcal{L}_1 \cup \mathcal{L}_2 + v = \mathcal{L}_1 \cup \mathcal{L}_2 \quad \Leftrightarrow \quad v = \begin{pmatrix} 0 \\ 0 \end{pmatrix}.$$

Assumption 1. *We assume from this point on that the lattices \mathcal{R}_1 and \mathcal{R}_2 are incommensurate, and that the dual lattices \mathcal{R}_1^* and \mathcal{R}_2^* are also incommensurate.*

Note that incommensurability of the dual lattices is not equivalent to incommensurability of the real space lattice; see, e.g., [31].

The Dirac points and orbital displacements are similarly rotated

$$K_1 := R\left(-\frac{\theta}{2}\right)K, \quad K_2 := R\left(\frac{\theta}{2}\right)K, \quad K'_j := -K_j,$$

$$\tau_{1\sigma} := R\left(-\frac{\theta}{2}\right)\tau_\sigma, \quad \tau_{2\sigma} := R\left(\frac{\theta}{2}\right)\tau_\sigma.$$

Let $\mathcal{A}_1 := \{1A, 1B\}$ and $\mathcal{A}_2 := \{2A, 2B\}$ be the set of indices of orbital displacements for sheet 1 and 2 respectively. Let $\Omega_j := \mathcal{R}_j \times \mathcal{A}_j$, then the full degree of freedom space is $\Omega := \Omega_1 \cup \Omega_2$. We write the wave functions in TBG by $\psi = (\psi_1, \psi_2)^T \in \oplus_{j=1}^2 \ell^2(\Omega_j)$, the incommensurate tight-binding model acts as

$$H\psi = \begin{pmatrix} H_{11} & H_{12} \\ H_{12}^\dagger & H_{22} \end{pmatrix} \begin{pmatrix} \psi_1 \\ \psi_2 \end{pmatrix}.$$

Here the intralayer part H_{jj} is similarly given by

$$(H_{jj})_{R\sigma, R'\sigma'} := h_{\sigma\sigma'}^{jj}(R - R'), \quad R\sigma, R'\sigma' \in \Omega_j, \quad j \in \{1, 2\},$$

with $h_{\sigma\sigma'}^{jj} : \mathcal{R}_j \rightarrow \mathbb{C}$, $h_{\sigma\sigma'}^{jj} \in \ell^1(\mathcal{R}_j)$, and the interlayer part H_{12} is given by

$$(H_{12})_{R\sigma, R'\sigma'} := h_{\sigma\sigma'}^{12}(R + \tau_\sigma - R' - \tau_{\sigma'}), \quad R\sigma \in \Omega_1, R'\sigma' \in \Omega_2,$$

with $h_{\sigma\sigma'}^{12} : \mathbb{R}^2 \rightarrow \mathbb{C}$, $h_{\sigma\sigma'}^{12} \in C(\mathbb{R}^2)$. We denote the Fourier transform pair by

$$(2.2) \quad \begin{aligned} \mathcal{F}h(\xi) &:= \hat{h}(\xi) := \int_{\mathbb{R}^2} e^{-ix \cdot \xi} h(x) dx \\ \mathcal{F}^{-1}\hat{h}(x) &:= \frac{1}{(2\pi)^2} \int_{\mathbb{R}^2} e^{ix \cdot \xi} \hat{h}(\xi) d\xi. \end{aligned}$$

We will employ the following assumption for interlayer hopping functions:

Assumption 2. *The interlayer hopping functions $h_{\sigma\sigma'}^{12} \in C(\mathbb{R}^2)$ for $\sigma \in \mathcal{A}_1, \sigma' \in \mathcal{A}_2$ satisfy for some $\gamma_{12}, \gamma'_{12} > 0$*

$$|h_{\sigma\sigma'}^{12}(x)| \lesssim e^{-\gamma_{12}|x|} \quad \forall x \in \mathbb{R}^2 \quad \text{and} \quad |\hat{h}_{\sigma\sigma'}^{12}(\xi)| \lesssim e^{-\gamma'_{12}|\xi|} \quad \forall \xi \in \mathbb{R}^2,$$

where we write $a \lesssim b$ to denote that there exists a constant $C > 0$ independent of parameters appearing on either the left or right-hand side so that $a \leq Cb$.

For intralayer, we use the following assumption:

Assumption 3. *The intralayer hopping functions $h_{\sigma\sigma'}^{jj} \in \ell^1(\mathcal{R}_j)$ for $\sigma, \sigma' \in \mathcal{A}_j$ satisfy for some $\gamma_j > 0$*

$$|h_{\sigma\sigma'}^{jj}(R)| \lesssim e^{-\gamma_j|R|} \quad \forall R \in \mathcal{R}_j.$$

We next describe the simplified model as a special case of the above structure. The intralayer and interlayer hopping functions arise in practice from overlap integrals of exponentially-decaying Wannier orbitals. A physically reasonable choice of such functions is therefore

$$(2.3) \quad h_{\sigma\sigma'}^{jj}(x) = e^{-\alpha|x+\tau_\sigma-\tau_{\sigma'}|}, \quad j \in \{1, 2\},$$

$$(2.4) \quad h_{\sigma\sigma'}^{12}(x) = h_{12}(x) = e^{-\beta\sqrt{|x|^2+z^2}},$$

for constants $\alpha, \beta, z > 0$. Here, z models the non-zero interlayer displacement. These functions clearly satisfy Assumptions 2 and 3; the Fourier transform of the interlayer hopping function is [1]

$$(2.5) \quad \hat{h}_{12}(\xi) = 2\pi \frac{\beta e^{-z\sqrt{|\xi|^2 + \beta^2}} \left(1 + z\sqrt{|\xi|^2 + \beta^2}\right)}{(|\xi|^2 + \beta^2)^{3/2}}.$$

More accurate forms for the functions (2.3)-(2.5) can be obtained from DFT calculations; this is the approach of [17], which we refer to as the Wannierized model. We provide computations using this model below.

2.3. Momentum Space. We now transform the real space Hamiltonian to the momentum space setting. We denote wave functions in the Bloch domain $L^2(\Gamma_j^*; \mathbb{C}^2)$ by $\tilde{\psi}_j = (\tilde{\psi}_j(q))_{q \in \Gamma_j^*} = ((\tilde{\psi}_j)_{jA}(q), (\tilde{\psi}_j)_{jB}(q))_{q \in \Gamma_j^*}^T$, and define unitary Bloch transforms in each layer by

$$(2.6) \quad \begin{aligned} [\mathcal{G}_j \psi_j]_\sigma(q) &:= \frac{1}{|\Gamma_j^*|^{1/2}} \sum_{R \in \mathcal{R}_j} e^{-iq \cdot (R + \tau_\sigma)} (\psi_j)_{R\sigma} \\ [\mathcal{G}_j^* \tilde{\psi}_j]_{R\sigma} &:= \frac{1}{|\Gamma_j^*|^{1/2}} \int_{\Gamma_j^*} e^{iq \cdot (R + \tau_\sigma)} \tilde{\psi}_{j\sigma}(q) dq, \end{aligned}$$

for $R\sigma \in \Omega_j$, $j \in \{1, 2\}$. Note that with this convention, Bloch transforms are quasi-periodic with respect to \mathcal{R}_j^* in the sense that

$$(2.7) \quad [\mathcal{G}_j \psi_j]_\sigma(q + G) = e^{-iG \cdot \tau_\sigma} [\mathcal{G}_j \psi_j]_\sigma(q), \quad G\sigma \in \mathcal{R}_j^* \times \mathcal{A}_j,$$

so the functions in $L^2(\Gamma_j^*; \mathbb{C}^2)$ can be defined over \mathbb{R}^2 . We denote momentum space bilayer wavefunctions by

$$(2.8) \quad \tilde{\psi} = (\tilde{\psi}_1, \tilde{\psi}_2)^T \in \oplus_{j=1}^2 L^2(\Gamma_j^*; \mathbb{C}^2).$$

Let $\mathcal{G} = (\mathcal{G}_1, \mathcal{G}_2)$, the momentum space Hamiltonian is defined via

$$(2.9) \quad H^{\text{ms}} \tilde{\psi} := \mathcal{G} H \mathcal{G}^* \tilde{\psi} = \begin{pmatrix} \mathcal{G}_1 H_{11} \mathcal{G}_1^* \tilde{\psi}_1 + \mathcal{G}_1 H_{12} \mathcal{G}_2^* \tilde{\psi}_2 \\ \mathcal{G}_2 H_{12}^\dagger \mathcal{G}_1^* \tilde{\psi}_1 + \mathcal{G}_2 H_{22} \mathcal{G}_2^* \tilde{\psi}_2 \end{pmatrix}.$$

Up to a phase change in the definition of the Bloch transform, the calculation from previous work [24] gives

$$(2.10) \quad \begin{aligned} [\mathcal{G}_j H_{jj} \mathcal{G}_j^*]_{\sigma\sigma'} &= \tilde{h}_{\sigma\sigma'}^{jj}(\cdot) := \sum_{R_j \in \mathcal{R}_j} e^{-i(\cdot) \cdot (R_j + \tau_\sigma - \tau_{\sigma'})} h_{\sigma\sigma'}^{jj}(R_j), \quad \sigma, \sigma' \in \mathcal{A}_j \\ [\mathcal{G}_1 H_{12} \mathcal{G}_2^*]_{\sigma\sigma'} &= c_1 c_2 \sum_{G \in \mathcal{R}_1^*} e^{iG \cdot \tau_\sigma} \hat{h}_{\sigma\sigma'}^{12}(\cdot + G) T_G, \quad \sigma \in \mathcal{A}_1, \sigma' \in \mathcal{A}_2 \end{aligned}$$

where $c_j := |\Gamma_j|^{-1/2}$, and T_G is the translation operator on $L^2(\Gamma_j^*; \mathbb{C}^2)$:

$$(T_G \tilde{\psi}_j)(q) = \tilde{\psi}_j(q + G).$$

Recalling that we assume incommensurability of the bilayer real space lattices (Assumption 1), using Birkhoff's ergodic theorem, a large class of observables associated to the momentum space Hamiltonian H^{ms} equal the same observables associated to a discrete "reciprocal space" Hamiltonian \hat{H} describing hopping on the bilayer reciprocal lattices. This perspective turns out to be the most convenient for justifying truncation of the Hamiltonian to a family of finite-dimensional matrices for numerical computation. In deriving the reciprocal space Hamiltonian we have to restrict attention to the class of analytic functions in momentum space, rather than considering the full L^2 space, so that we can consider pointwise values of the momentum space wavefunctions. Since when we evaluate observables we consider the trace over plane wave basis functions, which clearly belong to this space, this restriction is not significant.

We now derive the reciprocal space Hamiltonian following [23, 24]. Let \mathcal{X}_j be the space of analytic periodic functions in $L^2(\Gamma_j^*; \mathbb{C}^2)$, and $\Omega_j^* := \mathcal{R}_{\mathbb{F}_j}^* \times \mathcal{A}_j$ with $\mathbb{F}_1 := 2, \mathbb{F}_2 := 1$. We define a map $\mathcal{E}_{q,j} : \mathcal{X}_j \rightarrow \ell^\infty(\Omega_j^*)$ that takes functions defined over momenta to a discrete dense sampling of the function

$$\{\mathcal{E}_{q,j}\tilde{\psi}_j\}_{G\sigma} := \tilde{\psi}_{j\sigma}(q + G).$$

Let $\Omega^* = \Omega_1^* \cup \Omega_2^*$ and

$$\mathcal{E}_q := \begin{pmatrix} \mathcal{E}_{q,1} & 0 \\ 0 & \mathcal{E}_{q,2} \end{pmatrix},$$

the reciprocal space Hamiltonian $\hat{H}(q) : \ell^2(\Omega^*) \rightarrow \ell^2(\Omega^*)$ takes the form

$$(2.11) \quad \mathcal{E}_q(H^{\text{ms}}\tilde{\psi}) =: \hat{H}(q)\mathcal{E}_q\tilde{\psi}, \quad \tilde{\psi} \in \oplus_{j=1}^2 \mathcal{X}_j.$$

Likewise, $\hat{H}(q)$ can be denoted in a sheet-wise decomposition

$$(2.12) \quad \hat{H}(q) = \begin{pmatrix} \hat{H}_{11}(q) & \hat{H}_{12}(q) \\ \hat{H}_{12}^\dagger(q) & \hat{H}_{22}(q) \end{pmatrix},$$

with intralayer entries

$$[\hat{H}_{jj}(q)]_{G,G'} := \tilde{h}^{jj}(q + G)\delta_{GG'}, \quad G, G' \in \mathcal{R}_{\mathbb{F}_j}^*$$

and interlayer entries

$$[\hat{H}_{12}(q)]_{G,G'} := c_1 c_2 \mathbb{T}_{G,G'} \odot \hat{h}^{12}(q + G + G'), \quad G \in \mathcal{R}_2^*, G' \in \mathcal{R}_1^*.$$

Here $\mathbb{T}_{G,G'}^{\sigma\sigma'} := e^{iG'\cdot\tau_\sigma} e^{-iG\cdot\tau_{\sigma'}}$ is the phase matrix, and \odot is the Hadamard product operator so that for 2×2 matrices \mathbb{T}, \mathbb{S} and $\sigma \in \mathcal{A}_1, \sigma' \in \mathcal{A}_2$,

$$(\mathbb{T} \odot \mathbb{S})_{\sigma\sigma'} := (\mathbb{T})_{\sigma\sigma'} (\mathbb{S})_{\sigma\sigma'}.$$

We further express electronic observables via (2.12). The density of states (DoS) is approximated by the Gaussian smearing for the thermodynamic limit trace

$$(2.13) \quad D_\varepsilon(E) := \underline{\text{Tr}} \delta_\varepsilon(E - H) := \lim_{r \rightarrow \infty} \frac{1}{\#\Omega_r} \sum_{R\sigma \in \Omega_r} [\delta_\varepsilon(E - H)]_{R\sigma, R\sigma},$$

where $\delta_\varepsilon(E - \lambda) := \frac{1}{\varepsilon\sqrt{2\pi}}e^{-(E-\lambda)^2/2\varepsilon^2}$ is the Gaussian centered at $E \in \mathbb{R}$, and $\Omega_r := \{R\sigma \in \Omega : |R| < r\}$ is the restricted space with $r > 0$. The DoS can be re-expressed using an ergodic theorem from [24], which we state for reference:

Theorem 2.1. *Assume Assumption 1 and assume H has hopping functions satisfying Assumptions 2 and 3. Then we have*

$$(2.14) \quad D_\varepsilon(E) = \nu^* \sum_{j=1}^2 \sum_{\sigma \in \mathcal{A}_j} \int_{\Gamma_j^*} [\delta_\varepsilon(E - \widehat{H}(q))]_{0\sigma, 0\sigma} dq$$

with

$$\nu^* = \frac{1}{2} \left(\sum_{j=1}^2 |\Gamma_j^*| \right)^{-1}.$$

2.4. Reciprocal Space Truncation. We next review the algorithm that truncates the reciprocal space formulation (2.12) as a finite sparse matrix to make the problem computationally tractable and numerically efficient [23, 24]. When we are only interested in a specific range of energies, such as a small subset of the monolayer spectra, we can select a finite basis set based on the energy and momenta relationship arising from the monolayer band structure. Specifically, we define for an energy region $E \subset \mathbb{R}$ and $r > 0$, the corresponding momenta regions in Γ_j^*

$$\Gamma_j^*(E) := \left\{ q \in \Gamma_j^* : \sigma_j(q) \cap E \neq \emptyset \right\},$$

where $\sigma_j(q)$ is the set of eigenvalues of $\widehat{H}_{jj}(q)$, and the corresponding set of basis elements

$$\Omega_r^*(q, E) := \left\{ G\sigma \in \Omega_j^* : \text{mod}_j(q + G) \in \Gamma_j^*(E) + B_r(0), j = 1, 2 \right\},$$

where $B_r(0)$ is a ball in \mathbb{R}^2 of radius r centered at 0, set addition is defined as $U + V := \{u + v : u \in U, v \in V\}$, and mod_j denotes values modulo the reciprocal lattice of layer j . The set $\Omega_r^*(q, E)$ will generally be infinite because of incommensurability.

Here we are interested in the case of narrow energy regions centered at the Dirac energy in graphene, and small twist angles. In this case, for sufficiently small $r > 0$, Ω_r^* decomposes into finite subsets centered at the K or K' Dirac points, such that the distance between these subsets and their “replicas” arising from the modular arithmetic is proportional to inverse twist angle. This happens because, whenever G is a reciprocal lattice vector of one layer, the value of G modulo the other layer’s reciprocal lattice has length proportional to θ . In order to pick out the region containing the starting momentum q , we define the map $I : \mathcal{B}(\Omega^*) \rightarrow \mathcal{B}(\Omega^*)$ as the operation that maps a subset of Ω^* to its isolated degrees of freedom containing the site 0σ for any σ , where $\mathcal{B}(\Omega^*)$ is the collection of subsets of Ω^* .

Assume we are only interested in the energy region around Dirac points K, K' , i.e., $B_\Sigma := (-\Sigma, \Sigma)$, $\Sigma > 0$. We expand it by $B_{\Sigma+\eta} := (-\Sigma - \eta, \Sigma + \eta)$, with η is a little larger

than twice the interlayer coupling strength,

$$(2.15) \quad \eta := (2 + \alpha) \sup_{\psi \in \ell^2(\Omega^*)} \frac{1}{\|\psi^{(1)}\|_2 \|\psi^{(2)}\|_2} (\psi^{(1)}, 0) \hat{H}(q) \begin{pmatrix} 0 \\ \psi^{(2)} \end{pmatrix},$$

where $\alpha > 0$. The basis space corresponding to B_Σ is

$$(2.16) \quad \Omega_r^*(q) := I(\Omega_r^*(q, B_{\Sigma+\eta})).$$

Note that for $r = 0$, the momenta regions are bounded by the balls $B_{r_\Sigma}(\text{mod}_j(K_j))$ and $B_{r_\Sigma}(\text{mod}_j(K'_j))$ with

$$(2.17) \quad r_\Sigma := \max_{q \in \Gamma_j^*(B_{\Sigma+\eta})} \min_{\tilde{K}_j \in \{K_j, K'_j\}} |q - \text{mod}_j(\tilde{K}_j)|.$$

As an example for the relationship between energy, momenta regions and bounding balls, see Figure 2.2. Additionally, there exists $r_m > 0$ such that for $r + r_\Sigma > r_m$, $\Gamma_j^*(B_{\Sigma+\eta}) + B_r(0)$

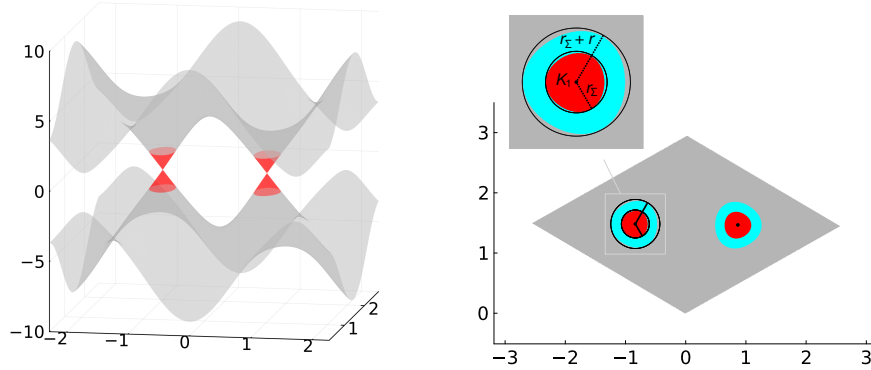


FIGURE 2.2. The left picture shows the rotated monolayer graphene band structure, where the red regions correspond to $B_{\Sigma+\eta}$. The right picture shows the reciprocal unit cell of the rotated monolayer graphene, where the red regions are $\Gamma_1^*(B_{\Sigma+\eta})$, and by adding the blue regions around them we obtain $\Gamma_1^*(B_{\Sigma+\eta}) + B_r(0)$. Here K_1 represents $\text{mod}_1(K_1)$.

becomes homotopically non-trivial [24]. Therefore, we should take $r < r_m - r_\Sigma$ to ensure a meaningful numerical scheme. It is also important to mention that if q is near K (K'), then $\Omega_r^*(q)$ only corresponds to the K (K') valley, if $\text{mod}_j(q) \notin \Gamma_j^*(B_{\Sigma+\eta}) + B_r(0)$, then $\Omega_r^*(q)$ is empty. We then define the inclusion map

$$(2.18) \quad J_{V \leftarrow U} : \ell^2(U) \rightarrow \ell^2(V), \quad U \subset V \subset \Omega^*,$$

and denote the inclusion of $\Omega_r^*(q)$ into Ω^* by $J_r(q) := J_{\Omega^* \leftarrow \Omega_r^*(q)}$. The corresponding finite matrix is $J_r^*(q) \hat{H}(q) J_r(q)$.

We further exploit the exponential decay of the interlayer hopping functions to sparsify the Hamiltonian matrix. Let $\tau \in \mathbb{Z}_+$ be a truncation parameter for hopping distance. We define the truncated hopping index set for $\tilde{K} \in \{K, K'\}$ valley by

$$\mathcal{B}_\tau := \left\{ n \in \mathbb{Z}^2 : |\tilde{K}_1 + 2\pi A_1^{-T} n| \text{ is among the } \tau \text{ smallest magnitudes of } \tilde{K}_1 + G_1 \right\}.$$

The size of the index set, $\#\mathcal{B}_\tau$, is $O(\tau^2)$. Interestingly, numerical computations suggest that $\#\mathcal{B}_\tau$ is close to $O(\tau)$, but we are not aware of any proof of this. Additionally, note that \mathcal{B}_τ for K' valley is the negative of \mathcal{B}_τ for K valley, since $K'_j = -K_j$. The restricted interlayer part is then given by

$$[\hat{H}_{12}^{(\tau)}(q)]_{G,G'} := [\hat{H}_{12}(q)]_{G,G'} \delta_{\mathcal{I}(G) + \mathcal{I}(G') \in \mathcal{B}_\tau},$$

where $\mathcal{I} : \mathcal{R}_1^* \cup \mathcal{R}_2^* \rightarrow \mathbb{Z}^2$ is the index map

$$\mathcal{I}(G_j) := A_j^T G_j / 2\pi, \quad G_j \in \mathcal{R}_j^*.$$

Finally, we construct the truncated matrix by

$$(2.19) \quad \hat{H}_r^{(\tau)}(q) := J_r^*(q) \begin{pmatrix} \hat{H}_{11}(q) & \hat{H}_{12}^{(\tau)}(q) \\ \left(\hat{H}_{12}^{(\tau)}(q)\right)^\dagger & \hat{H}_{22}(q) \end{pmatrix} J_r(q).$$

The DoS of H at $E \in B_\Sigma$ can be well approximated by the DoS of $\hat{H}_r^{(\tau)}$, when there is a large moiré pattern, which occurs at small twist angle θ . We require the following definition for moiré-periodic systems.

Definition 2.2. *The moiré reciprocal lattice and moiré Brillouin zone are*

$$\mathcal{R}_M^* := 2\pi\Theta\mathbb{Z}^2, \quad \Gamma_M^* := 2\pi\Theta[0,1)^2$$

with lattice matrix

$$\Theta := A_2^{-T} - A_1^{-T}.$$

The moiré Dirac points are

$$K_M := K_1, \quad K'_M := K_2.$$

We also define the maps $\mathfrak{G}_j : \mathcal{R}_M^* \rightarrow \mathcal{R}_j^*$ and $\mathfrak{G}_M : \mathcal{R}_1^* \cup \mathcal{R}_2^* \rightarrow \mathcal{R}_M^*$ as transformations between moiré reciprocal lattices and monolayer reciprocal lattices

$$(2.20) \quad \begin{aligned} \mathfrak{G}_j(G_M) &:= A_j^{-T} \Theta^{-1} G_M, & G_M \in \mathcal{R}_M^*, \\ \mathfrak{G}_M(G_j) &:= (-1)^j \Theta A_j^T G_j, & G_j \in \mathcal{R}_j^*. \end{aligned}$$

Using periodicity of $\hat{H}_r^{(\tau)}(\cdot)$ with respect to moiré reciprocal lattices up to unitary transformation, the starting momenta in (2.14) can be restricted into the much smaller space Γ_M^* [23]. We restate the result for reference:

Theorem 2.2. *Assume Assumption 1 and assume TBG has hopping functions satisfying Assumptions 2 and 3. We define DoS for the truncated Hamiltonian at valley $\tilde{K} \in \{K, K'\}$ by*

$$(2.21) \quad D_{\varepsilon,r}^{(\tau)}(E; \tilde{K}) := \nu^* \int_{\tilde{K} + \Gamma_M^*} \text{Tr} \, \delta_\varepsilon(E - \hat{H}_r^{(\tau)}(q)) \, dq.$$

Consider $E \in B_\Sigma$, $\theta \ll 1$, and $\varepsilon \ll 1$. Let $d_\tau \in \mathbb{R}_+$ be the hopping truncation distance depending on $\tau \in \mathbb{Z}_+$. Then there are constants γ_h , γ_m , and γ_g corresponding to hopping truncation error, momentum truncation error, and Gaussian decay rates respectively such that

$$(2.22) \quad \left| D_\varepsilon(E) - \sum_{\tilde{K} \in \{K, K'\}} D_{\varepsilon,r}^{(\tau)}(E; \tilde{K}) \right| \lesssim \varepsilon^{-2} e^{-\gamma_h d_\tau} + \varepsilon^{-4} e^{-\gamma_m r} + \varepsilon^{-1} e^{-\gamma_g \varepsilon^{-2}},$$

where $D_\varepsilon(E)$ is defined in (2.13) (equivalently (2.14)). Further, γ_m scales as θ^{-1} .

Note that the trace in (2.21) converges trivially since $\hat{H}_r^{(\tau)}(q)$ is a finite-dimensional matrix. Estimate (2.22) shows that the error on the right-hand side is small when d_τ and r are large and ε is small, as long as ε does not $\downarrow 0$ too fast. Specifically, as long as

$$(2.23) \quad \varepsilon \gg e^{-\frac{1}{4}\gamma_m r}, \quad \varepsilon \gg e^{-\frac{1}{2}\gamma_h d_\tau},$$

then the error in (2.22) will $\rightarrow 0$ as $\varepsilon \downarrow 0$ and $r, d_\tau \rightarrow \infty$. It is important to note that increasing r beyond a certain value will result in an infinite-dimensional “truncated” matrix, which cannot be diagonalized exactly. However, in practice, the error in (2.22) becomes very small for small ε well before this point.

3. DERIVATION OF CONTINUUM MODELS FROM TRUNCATED RECIPROCAL SPACE MODELS

In this section, we will propose an approximation scheme to obtain the higher order continuum models. As seen in Figure 3.3, we have obtained the truncated Hamiltonian $\hat{H}_r^{(\tau)}$ by the Bloch transform, an unfolding procedure, and the reciprocal space truncation in Section 2. The next step is to perform the Taylor expansion at the Dirac points of the incommensurate Brillouin zone to obtain a polynomial approximation Hamiltonian $\hat{H}_r^{(m,n,\tau)}$. Subsequently, we will use a similar inverse process to derive the continuum model, including an infinite extension to define the Hamiltonian on \mathbb{R}^2 , a folding process back to the momentum space, and the inverse Fourier transform to obtain the PDE form.

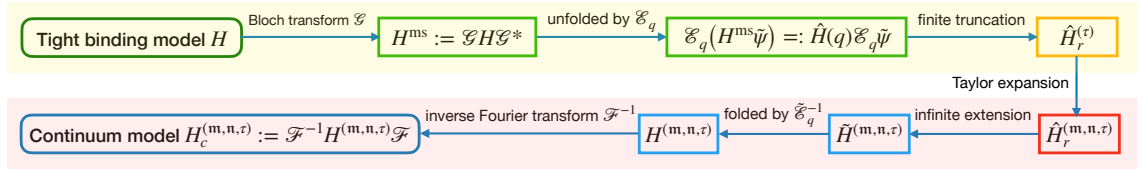


FIGURE 3.3. Procedure for the construction of the continuum model.

3.1. Taylor Expansion. We begin with a momenta polynomial approximation of (2.19). We note that the DoS (2.21) is an integral over the moiré Brillouin zone Γ_M^* . We hence can only consider the behavior of the Hamiltonian in moiré reciprocal space. We rewrite (2.19) by the moiré reciprocal lattices and do the Taylor expansion around $\tilde{K} \in \{K, K'\}$ valley to obtain the polynomial approximation model.

Before expanding the Hamiltonian, we introduce the 2-dimensional multi-index notations for $\beta \in \mathbb{N}^2$, $\xi \in \mathbb{R}^2$ and $h : \mathbb{R}^2 \rightarrow \mathbb{C}$, $h \in C(\mathbb{R}^2)$,

$$|\beta| := \beta_1 + \beta_2, \quad \beta! := \beta_1! \beta_2!, \quad \xi^\beta := \xi_1^{\beta_1} \xi_2^{\beta_2}, \quad D^\beta h := \frac{\partial^{|\beta|} h}{\partial \xi_1^{\beta_1} \partial \xi_2^{\beta_2}}.$$

Let $\mathbf{m} \in \mathbb{N}$ and $\mathbf{n} \in \mathbb{N}$ be the intralayer and interlayer expansion orders, respectively. For $G\sigma, G'\sigma' \in \Omega_j^*$, we do the Taylor expansion for \tilde{h}^{jj} with respect to $q + \mathfrak{G}_M(G)$ around \tilde{K}_j ,

$$\begin{aligned} \tilde{h}_{\sigma\sigma'}^{jj}(q + G) &= e^{-i(G - \mathfrak{G}_M(G)) \cdot (\tau_\sigma - \tau_{\sigma'})} \tilde{h}_{\sigma\sigma'}^{jj}(q + \mathfrak{G}_M(G)) \\ &\approx e^{-i(G - \mathfrak{G}_M(G)) \cdot (\tau_\sigma - \tau_{\sigma'})} P_{j,\sigma\sigma'}^{\mathbf{m}}(q - \tilde{K}_j + \mathfrak{G}_M(G)), \end{aligned}$$

where we denote the \mathbf{m} -order Taylor polynomial approximation of $\tilde{h}_{\sigma\sigma'}^{jj}$ by

$$(3.24) \quad P_{j,\sigma\sigma'}^{\mathbf{m}}(\xi) := \sum_{|\beta| \leq \mathbf{m}} \frac{D^\beta \tilde{h}_{\sigma\sigma'}^{jj}(\tilde{K}_j)}{\beta!} \xi^\beta.$$

For $G\sigma \in \Omega_1^*$, $G'\sigma' \in \Omega_2^*$, let

$$\tilde{G}_1 := G + G' - \mathfrak{G}_M(G) \in \mathcal{R}_1^*,$$

we do the Taylor expansion for \hat{h}^{12} with respect to $q + \mathfrak{G}_M(G) + \tilde{G}_1$ around $\tilde{K}_1 + \tilde{G}_1$,

$$\begin{aligned} c_1 c_2 \hat{h}_{\sigma\sigma'}^{12}(q + G + G') \delta_{\mathcal{I}(G) + \mathcal{I}(G') \in \mathcal{B}_\tau} &= c_1 c_2 \hat{h}_{\sigma\sigma'}^{12}(q + \mathfrak{G}_M(G) + \tilde{G}_1) \delta_{\mathcal{I}(\tilde{G}_1) \in \mathcal{B}_\tau} \\ &\approx U_{\tilde{G}_1, \sigma\sigma'}^{\mathbf{n}}(q - \tilde{K}_1 + \mathfrak{G}_M(G)) \delta_{\mathcal{I}(\tilde{G}_1) \in \mathcal{B}_\tau} \end{aligned}$$

where we denote the \mathbf{n} -order Taylor polynomial approximation of $c_1 c_2 \hat{h}_{\sigma\sigma'}^{12}$ by

$$(3.25) \quad U_{\tilde{G}_1, \sigma\sigma'}^{\mathbf{n}}(\xi) := c_1 c_2 \sum_{|\beta| \leq \mathbf{n}} \frac{D^\beta \hat{h}_{\sigma\sigma'}^{12}(\tilde{K}_1 + \tilde{G}_1)}{\beta!} \xi^\beta.$$

Hence, the polynomial approximation Hamiltonian is given by

$$(3.26) \quad \hat{H}_r^{(\mathbf{m}, \mathbf{n}, \tau)}(q) := J_r^*(q) \begin{pmatrix} \hat{H}_{11}^{(\mathbf{m})}(q) & \hat{H}_{12}^{(\mathbf{n}, \tau)}(q) \\ \left(\hat{H}_{12}^{(\mathbf{n}, \tau)}(q)\right)^\dagger & \hat{H}_{22}^{(\mathbf{m})}(q) \end{pmatrix} J_r(q),$$

where

$$[\hat{H}_{jj}^{(\mathbf{m})}(q)]_{G\sigma, G'\sigma'} := e^{-i(G - \mathfrak{G}_M(G)) \cdot (\tau_\sigma - \tau_{\sigma'})} P_{j,\sigma\sigma'}^{\mathbf{m}}(q - \tilde{K}_j + \mathfrak{G}_M(G)) \delta_{GG'},$$

and

$$[\hat{H}_{12}^{(\mathbf{n}, \tau)}(q)]_{G\sigma, G'\sigma'} := \mathbb{T}_{G, G'}^{\sigma\sigma'} U_{\tilde{G}_1, \sigma\sigma'}^{\mathbf{n}}(q - \tilde{K}_1 + \mathfrak{G}_M(G)) \delta_{\mathcal{I}(\tilde{G}_1) \in \mathcal{B}_\tau}.$$

We note that for $q \in \tilde{K} + \Gamma_M^*$ and $G\sigma \in \Omega_r^*(q)$, we have $|q - \tilde{K}_j + \mathfrak{G}_M(G)| \leq r_\Sigma + r$, $G \in \mathcal{R}_{F_j}^*$. Since the Taylor expansion error scales as $O(|q - \tilde{K}_j + \mathfrak{G}_M(G)|^{j+1})$, $j = \mathbf{m}, \mathbf{n}$, the expansion accuracy will also be determined by the reciprocal space truncation. The following lemma gives the precise error analysis of the polynomial approximation.

Lemma 3.1. *Assume Assumption 1 and assume TBG has hopping functions satisfying Assumption 2 and 3. For $q \in \tilde{K} + \Gamma_M^*$, $\tilde{K} \in \{K, K'\}$, $\theta \ll 1$, and $r < \min\{\gamma_1, \gamma_2, \gamma_{12}, r_m\} - r_\Sigma$, there is a constant C independent of $\mathbf{m}, \mathbf{n}, \tau$, such that the error of the polynomial approximation is*

$$(3.27) \quad \|\hat{H}_r^{(\tau)}(q) - \hat{H}_r^{(\mathbf{m}, \mathbf{n}, \tau)}(q)\|_{\text{op}} \leq C \left((\mathbf{m}+1) \left(\max_{j=1,2} \gamma_j^{-1}(r_\Sigma + r) \right)^{\mathbf{m}+1} + \#\mathcal{B}_\tau(\mathbf{n}+1) (\gamma_{12}^{-1}(r_\Sigma + r))^{\mathbf{n}+1} \right).$$

Proof. Proof is in Appendix A. \square

Estimate (3.27) in particular implies convergence of the DoS of the polynomially approximated Hamiltonian $\hat{H}_r^{(\mathbf{m}, \mathbf{n}, \tau)}$ to that of $\hat{H}_r^{(\tau)}$. Combining this result with Theorem 2.2 will allow us to relate the DoS of $\hat{H}_r^{(\mathbf{m}, \mathbf{n}, \tau)}$ with the full DoS (2.13) in our main result Theorem 3.1.

3.2. Continuum Model. We now derive the continuum model from (3.26). It is not immediately obvious how to do this, as $\hat{H}_r^{(\mathbf{m}, \mathbf{n}, \tau)}$ is defined on $\Gamma_j^*(B_{\Sigma+\eta}) + B_r(0)$ (see the momentum domain in the polynomial expansion), while the continuum model is defined on \mathbb{R}^2 . However, we find that the density of states of these models can be related as long as we focus on low energies, i.e., energies close to the monolayer Dirac energy. To make this precise, we have to extend the Hamiltonian to all of \mathbb{R}^2 in such a way that it remains unchanged for small momenta (i.e., momenta close to the monolayer Dirac point) but becomes invertible for large momenta. We will then apply the inverse Fourier transform to obtain the continuum model.

For $\tilde{K} \in \{K, K'\}$, let $\tilde{\chi}_r(\xi) := \xi \chi_r(\xi)$ with $\chi_r(\xi)$ smooth and 1 on

$$\bigcup_{j=1,2} \left\{ \left\{ \Gamma_j^*(B_{\Sigma+\eta}) + B_r(0) + \tilde{K}_j - \text{mod}_j(\tilde{K}_j) \right\} \cap B_{r_\Sigma+r}(\tilde{K}_j) \right\},$$

and compactly supported on

$$\bigcup_{j=1,2} \left\{ \left\{ \Gamma_j^*(B_{\Sigma+\eta}) + B_{r'}(0) + \tilde{K}_j - \text{mod}_j(\tilde{K}_j) \right\} \cap B_{r_\Sigma+r'}(\tilde{K}_j) \right\},$$

with $0 < r' - r \ll 1$ so that the momenta extended by r' do not contribute to the DoS. Here $\tilde{K}_j - \text{mod}_j(\tilde{K}_j)$ shifts the momenta in the Brillouin zone to the reciprocal lattice unit cell containing \tilde{K}_j , and the intersection ensures that the momenta correspond to \tilde{K} (see Figure 2.2). We modify the expansion polynomials by

$$(3.28) \quad \tilde{P}_j^{\mathbf{m}}(\xi) := P_j^1(\xi) + (P_j^{\mathbf{m}} - P_j^1)(\tilde{\chi}_r(\xi)), \quad \tilde{U}_{G_1}^{\mathbf{n}}(\xi) := U_{G_1}^{\mathbf{n}}(\tilde{\chi}_r(\xi)),$$

and denote the corresponding Hamiltonian parts by $\tilde{H}_{jj}^{(m)}$ and $\tilde{H}_{12}^{(n,\tau)}$. Then the infinite matrix is

$$\tilde{H}^{(m,n,\tau)}(q) := \begin{pmatrix} \tilde{H}_{11}^{(m)}(q) & \tilde{H}_{12}^{(n,\tau)}(q) \\ \left(\tilde{H}_{12}^{(n,\tau)}(q)\right)^\dagger & \tilde{H}_{22}^{(m)}(q) \end{pmatrix}.$$

The reason for modifying the expansion polynomials as in (3.28) is to ensure that \tilde{P}_j^m is invertible for large $|\xi|$, which will be important in the proofs below.

We notice that $\tilde{H}^{(m,n,\tau)}$ could be rewritten by the moiré reciprocal lattice, i.e., for $G_M\sigma, G'_M\sigma' \in \Omega_{jM}^* := \mathcal{R}_M^* \times \mathcal{A}_j$,

$$(3.29) \quad [\tilde{H}_{jj}^{(m)}(q)]_{G_M\sigma, G'_M\sigma'} = e^{i\mathfrak{G}_j(G_M) \cdot (\tau_{\sigma'} - \tau_\sigma)} \tilde{P}_{j,\sigma\sigma'}^m(q - \tilde{K}_j + (-1)^{F_j} G_M) \delta_{G_M G'_M},$$

and for $G_M\sigma \in \Omega_{1M}^*, G'_M\sigma' \in \Omega_{2M}^*$,

$$(3.30) \quad [\tilde{H}_{12}^{(n,\tau)}(q)]_{G_M\sigma, G'_M\sigma'} = \mathbb{T}_{\mathfrak{G}_2(G_M), \mathfrak{G}_1(G'_M)}^{\sigma\sigma'} \tilde{U}_{\mathfrak{G}_1(\tilde{G}_M), \sigma\sigma'}^n(q - \tilde{K}_1 + G_M) \delta_{\mathcal{I}(\tilde{G}_M) \in \mathcal{B}_\tau},$$

where $\tilde{G}_M := G_M + G'_M$ and $\mathcal{I}(G_M) := (2\pi\Theta)^{-1}G_M$ for $G_M \in \mathcal{R}_M^*$. We then define a map $\tilde{\mathcal{E}}_{q,j} : \mathcal{X}_j \rightarrow \ell^\infty(\Omega_{jM}^*)$ analogous to \mathcal{E}_q but sampled by moiré reciprocal lattices

$$\{\tilde{\mathcal{E}}_{q,j} \tilde{\psi}_j\}_{G_M\sigma} := e^{-i\mathfrak{G}_j(G_M) \cdot \tau_\sigma} \tilde{\psi}_j^\sigma(q - \tilde{K}_j + (-1)^{F_j} G_M),$$

and let

$$\tilde{\mathcal{E}}_q := \begin{pmatrix} \tilde{\mathcal{E}}_{q,1} & 0 \\ 0 & \tilde{\mathcal{E}}_{q,2} \end{pmatrix}.$$

The following lemma gives the folded (momentum space) form of the approximation model.

Lemma 3.2. *We construct the operator $H^{(m,n,\tau)} : \mathcal{F}H^1(\mathbb{R}^2; \mathbb{C}^4) \rightarrow L^2(\mathbb{R}^2; \mathbb{C}^4)$, where \mathcal{F} is the Fourier transform, decomposed sheet-wise as*

$$(3.31) \quad H^{(m,n,\tau)} = \begin{pmatrix} H_{11}^{(m)} & H_{12}^{(n,\tau)} \\ \left(H_{12}^{(n,\tau)}\right)^\dagger & H_{22}^{(m)} \end{pmatrix}$$

to be the Hamiltonian such that for $\tilde{\psi} \in \oplus_{j=1}^2 \mathcal{X}_j$,

$$\tilde{\mathcal{E}}_q(H^{(m,n,\tau)} \tilde{\psi}) = \tilde{H}^{(m,n,\tau)}(q) \tilde{\mathcal{E}}_q \tilde{\psi}.$$

The operator $H^{(m,n,\tau)}$ is composed of translation operators and multiplication operators given by

$$(3.32) \quad H_{jj}^{(m)} = \tilde{P}_j^m(\cdot), \quad j = 1, 2,$$

$$(3.33) \quad H_{12}^{(n,\tau)} = \sum_{\mathcal{I}(G_M) \in \mathcal{B}_\tau} \mathbb{T}_{G_M} \odot \tilde{U}_{\mathfrak{G}_1(G_M)}^n(\cdot) T_{s_{G_M}},$$

where $\mathbb{T}_{G_M}^{\sigma\sigma'} := e^{i\mathfrak{G}_1(G_M) \cdot \tau_\sigma} e^{-i\mathfrak{G}_2(G_M) \cdot \tau_{\sigma'}}$ for $\sigma \in \mathcal{A}_1, \sigma' \in \mathcal{A}_2$ and $s_{G_M} := \tilde{K}_1 - \tilde{K}_2 - G_M$.

Proof. See Appendix B. □

Finally, let $D := -i(\partial_{x_1}, \partial_{x_2})$ and $\tilde{\chi}_r^n(D)f(x) := \frac{1}{(2\pi)^2} \int_{\mathbb{R}^2} e^{i\xi x} \tilde{\chi}_r^n(\xi) \hat{f}(\xi) d\xi$. By the inverse Fourier transform, we obtain the continuum model for the \tilde{K} valley

(3.34)

$$H_c^{(\mathbf{m}, \mathbf{n}, \tau)} := \mathcal{F}^{-1} H^{(\mathbf{m}, \mathbf{n}, \tau)} \mathcal{F} = \begin{pmatrix} \tilde{P}_1^{\mathbf{m}}(D) & \sum_{\mathcal{I}(G_M) \in \mathcal{B}_\tau} \mathbb{T}_{G_M} \odot \tilde{U}_{\mathfrak{G}_1(G_M)}^{\mathbf{n}}(D - s_{G_M}) e^{-is_{G_M} \cdot x} \\ \sum_{\mathcal{I}(G_M) \in \mathcal{B}_\tau} \mathbb{T}_{G_M}^\dagger \odot \overline{\tilde{U}_{\mathfrak{G}_1(G_M)}^{\mathbf{n}}(D - s_{G_M})} e^{is_{G_M} \cdot x} & \tilde{P}_2^{\mathbf{m}}(D) \end{pmatrix}.$$

We refer to this as the $(\mathbf{m}, \mathbf{n}, \tau)$ continuum model. We mention that the r dependence is omitted in the continuum model Hamiltonian. This is because r is mainly used to improve numerical efficiency, and is always chosen to ensure the momentum truncation converges. Therefore, r does not fundamentally affect the accuracy of the continuum model.

In the following example, we can see that the BM model is a leading order continuum model. Therefore, we also refer to the $(1, 0, 1)$ continuum model as the BM model.

Example 3.1. *We consider the simplified TBG model in [32]. This simplified model has three nearest hoppings for the intralayer, and with a radial decay function for the interlayer such as (2.4). Specifically, the reciprocal space Hamiltonian for this model is*

(3.35)

$$[\hat{H}_{jj}]_{G, G'} = -t \begin{pmatrix} 0 & F_j(\cdot + G) \\ F_j(\cdot + G) & 0 \end{pmatrix} \delta_{GG'}, \quad F_j(q) := e^{iq \cdot (\tau_{jB} - \tau_{jA})} (1 + e^{-iq \cdot a_{j,1}} + e^{-iq \cdot a_{j,2}}),$$

$$[\hat{H}_{12}]_{G, G'} = c_1 c_2 \hat{h}_{12}(\cdot + G + G') \mathbb{T}_{G, G'}.$$

We first derive the $(1, 0, 1)$ continuum model for the K valley. We can easily obtain that

$$P_j^1(q) = v \sigma_{\theta_j} \cdot q, \quad \sigma_{\theta_j} \cdot q := \begin{pmatrix} 0 & e^{i\theta_j}(q_1 - iq_2) \\ e^{-i\theta_j}(q_1 + iq_2) & 0 \end{pmatrix}, \quad v := \frac{\sqrt{3}}{2} at, \quad \theta_j := (-1)^j \frac{\theta}{2},$$

and

$$U_{\tilde{G}_1}^0(q) = w \begin{pmatrix} 1 & 1 \\ 1 & 1 \end{pmatrix}, \quad w := c_1 c_2 \hat{h}_{12}(K_1 + \tilde{G}_1), \quad \mathcal{I}(\tilde{G}_1) \in \mathcal{B}_1,$$

where $\mathcal{B}_1 = \{(0, 0), (0, 1), (-1, 0)\}$. Here we use w as the interlayer coupling since the three nearest hopping terms have equal strength. Then we have

$$H_c^{(1, 0, 1)} = \begin{pmatrix} v \sigma_{-\theta/2} \cdot D & w \sum_{j=1}^3 \mathbb{T}_j e^{-is_j \cdot x} \\ \overline{w} \sum_{j=1}^3 \mathbb{T}_j^\dagger e^{is_j \cdot x} & v \sigma_{\theta/2} \cdot D \end{pmatrix},$$

where the matrices are

$$\mathbb{T}_1 := \begin{pmatrix} 1 & 1 \\ 1 & 1 \end{pmatrix}, \quad \mathbb{T}_2 := \begin{pmatrix} 1 & e^{-i\phi} \\ e^{i\phi} & 1 \end{pmatrix}, \quad \mathbb{T}_3 := \begin{pmatrix} 1 & e^{i\phi} \\ e^{-i\phi} & 1 \end{pmatrix},$$

with $\phi = 2\pi/3$, and the vectors are

$$s_1 := K_1 - K_2, \quad s_2 := K_1 - K_2 - 2\pi\Theta(0, 1)^T, \quad s_3 := K_1 - K_2 - 2\pi\Theta(-1, 0)^T.$$

The three vectors could also be explicitly given by

$$s_1 = |\Delta K|(0, -1)^T, \quad s_2 = |\Delta K|\left(\frac{\sqrt{3}}{2}, \frac{1}{2}\right)^T, \quad s_3 = |\Delta K|\left(-\frac{\sqrt{3}}{2}, \frac{1}{2}\right)^T,$$

where $|\Delta K| := 2|K|\sin(\theta/2)$ is the distance between the Dirac points of the layers. We can see that $H_c^{(1,0,1)}$ for the K valley is highly similar to the BM model given in [7].

Observe that $K' = -K$, we can immediately obtain the $(1, 0, 1)$ continuum model for the K' valley

$$H_c^{(1,0,1)} = \begin{pmatrix} v\sigma'_{-\theta/2} \cdot D & w \sum_{j=1}^3 \mathbb{T}'_j e^{-is'_j \cdot x} \\ \bar{w} \sum_{j=1}^3 \mathbb{T}'_j e^{is'_j \cdot x} & v\sigma'_{\theta/2} \cdot D \end{pmatrix},$$

where

$$(\sigma'_{\theta_j} \cdot q)_{\sigma\sigma'} := -\overline{(\sigma_{\theta_j} \cdot q)_{\sigma\sigma'}}, \quad (\mathbb{T}'_j)_{\sigma\sigma'} := \overline{(\mathbb{T}_j)_{\sigma\sigma'}}, \quad s'_j := -s_j.$$

3.3. Convergence of the Density of States. We finally discuss the convergence of the density of states of the continuum model. Similar with (2.21), that is approximated by

$$(3.36) \quad D_\varepsilon^{(\mathbf{m}, \mathbf{n}, \tau)}(E; \tilde{K}) := \nu^* \int_{\tilde{K} + \Gamma_M^*} \text{Tr} \delta_\varepsilon(E - \tilde{H}^{(\mathbf{m}, \mathbf{n}, \tau)}(q)) dq.$$

We can see that the error of $D_\varepsilon^{(\mathbf{m}, \mathbf{n}, \tau)}$ comes from three parts: truncation error, polynomial approximation error, and smooth extension error. The first one has been given by Theorem 2.2, the second one can be estimated by Lemma 3.1, and the last one can be analyzed using the “ring decomposition technique” proposed by [24].

Theorem 3.1. Assume Assumption 1 and assume TBG has hopping functions satisfying Assumption 2 and 3. Consider $E \in B_\Sigma$, $\theta \ll 1$, and $\varepsilon \ll 1$. Let $d_\tau \in \mathbb{R}_+$ be the hopping truncation distance depending on $\tau \in \mathbb{Z}_+$. Let $\mathbf{m}, \mathbf{n} \in \mathbb{N}$ be the intralayer and interlayer expansion orders respectively. Then for $r < \min\{\gamma_1, \gamma_2, \gamma_{12}, r_m\} - r_\Sigma$, there are constants γ_h , γ_m , and γ_g corresponding to hopping truncation error, momenta truncation error, and Gaussian decay rates respectively, such that

(3.37)

$$\begin{aligned} |D_\varepsilon(E) - \sum_{\tilde{K} \in \{K, K'\}} D_\varepsilon^{(\mathbf{m}, \mathbf{n}, \tau)}(E; \tilde{K})| &\leq C_{\Sigma, \theta, \tau, r} \left(\varepsilon^{-2} e^{-\gamma_h d_\tau} + \varepsilon^{-4} e^{-\gamma_m r} + \varepsilon^{-1} e^{-\gamma_g \varepsilon^{-2}} \right) \\ &\quad + \varepsilon^{-2} C_{\Sigma, \theta} \left((\mathbf{m} + 1) \left(\max_{j=1,2} \gamma_j^{-1} (r_\Sigma + r) \right)^{\mathbf{m}+1} + \#\mathcal{B}_\tau(\mathbf{n} + 1) (\gamma_{12}^{-1} (r_\Sigma + r))^{\mathbf{n}+1} \right), \end{aligned}$$

where $C_{\Sigma, \theta, \tau, r}$ is a constant dependent of Σ, θ, τ, r , and $C_{\Sigma, \theta}$ is a constant dependent of Σ, θ

$$(3.38) \quad C_{\Sigma, \theta} := C \max_{\tilde{K} \in \{K, K'\}} \#\Omega_0^*(\tilde{K}).$$

Proof. Proof is in Appendix C. \square

We note that the constant for the polynomial approximation error $C_{\Sigma,\theta}$ scales as $O(\Sigma\theta^{-2})$. Although we consider $\theta \ll 1$, since we only focus on a very small energy region around Dirac points, $C_{\Sigma,\theta}$ is still a small constant. We note as long as the hopping functions do not have asymptotic behavior with θ as is the case for the simplified and Wannier tight-binding models we consider, then $\gamma_m \sim \theta^{-1}$. Hence we can have r proportional to θ , and r_Σ is small as interlayer tunneling is weak in Van der Waals systems. Consequently, small Taylor expansion orders \mathbf{m}, \mathbf{n} are sufficient to ensure convergence. We mention that the inclusion of mechanical relaxation effects alters this asymptotic [23].

4. NUMERICAL SIMULATIONS

In this section, we shall give the high accuracy continuum models for the simplified TBG and the Wannierized TBG. We will demonstrate the conclusions by convergence results and band structures at the K valley for the magic angle ($\theta = 1.1^\circ$). The results are similar for the K' valley. For the simplified TBG, we consider the model given by (3.35) and use the tight-binding parameters given in [7] and [32]. For the Wannierized TBG, we consider the monolayer tight-binding hopping parameters up to the fourth nearest neighbor, with values obtained from a previous first-principles study of graphene [17], and interlayer hopping coupling is also derived from the first-principles calculations [17]. As seen in Figure 4.4, the interlayer hopping couplings of these two TBG models have different decay and symmetry. Therefore, we can anticipate that their BM models will exhibit different accuracy on the band structure near the flat band, and their high-order corrections are also different.

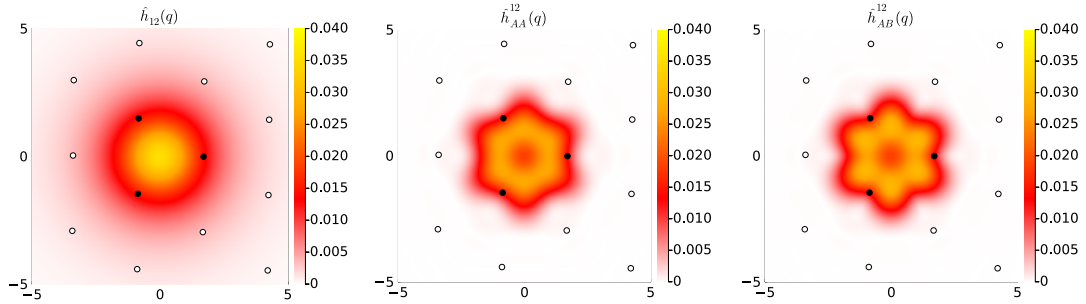


FIGURE 4.4. Magnitude of interlayer coupling in momentum space for the simplified TBG, AA and AB parts of the Wannierized TBG, respectively. The balls represent all $K_1 + G_1$, where the black balls are hoppings corresponding to \mathcal{B}_1 .

In particular, we will use a more succinct method to truncate the reciprocal space for TBG. Let $\Lambda > 0$ be the new momentum truncation parameter, then the basis set could be described by a fixed truncation radius

$$\Omega_\Lambda^* := \{G\sigma \in \Omega^* : |\mathfrak{G}_M(G)| < \Lambda\},$$

and the corresponding inclusion is $J_\Lambda := J_{\Omega^* \leftarrow \Omega_\Lambda^*}$. The reason for this is that the conical bands of graphene lead to a linear relationship between momentum cutoffs and energy range. We denote the high-symmetry lines of the moiré Brillouin zone at a single moiré K_M valley by L_{BZ} ($K_M \rightarrow \Gamma_M \rightarrow M_M \rightarrow K_M$), and define the relative error for momentum truncation along L_{BZ} by

$$\text{Err}(\Lambda, \Sigma) := \max_{\substack{q \in L_{BZ} \\ j: |\epsilon_j(q)| \leq \Sigma}} |\epsilon_j(q) - \epsilon_j(\Lambda, q)|,$$

where $\epsilon_j(q)$ and $\epsilon_j(\Lambda, q)$ are the j -th eigenvalues of $\hat{H}(q)$ and $J_\Lambda^* \hat{H}(q) J_\Lambda$, respectively. In Figure 4.5, we show the relative error as a bi-variate function of Λ and Σ for the Wannierized TBG. We can observe that Λ grows linearly with Σ when converging, which validates the rational choice of Ω_Λ^* . We also note that the error does not decrease continuously with Λ , this is because the cardinality of Ω_Λ^* increases piecewisely with Λ . In the following, all the

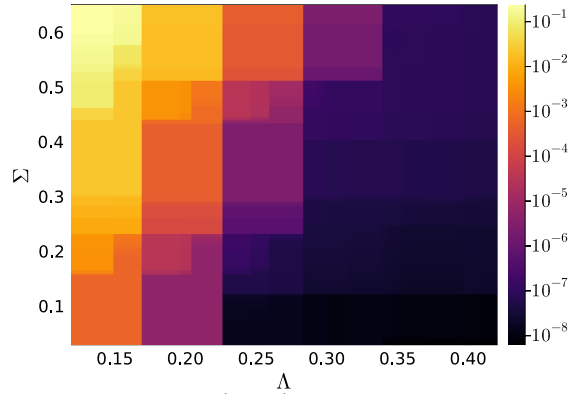


FIGURE 4.5. Relative error $\text{Err}(\Lambda, \Sigma)$ for the Wannierized TBG at $\theta = 1.1^\circ$.

simulations will use Ω_Λ^* as the momentum truncation basis set. Since we are only concerned with the parameters selection for the continuum model, we will omit the subscript of momentum truncation r/Λ (chosen to ensure the momentum truncation error converges) to simplify the notation.

To select the “optimal” parameters for high accuracy models, we need to know the contribution of each parameter to convergence. Therefore, we first use the momentum space model \hat{H} as a reference and compare it with $\hat{H}^{(\tau)}$ to evaluate the hopping truncation error. Next, we fix the hopping truncation parameter $\tau = \tau_0$, and compare $\hat{H}^{(\tau_0)}$ with $\hat{H}^{(\mathbf{m}, \infty, \tau_0)}$ ($\hat{H}^{(\infty, \mathbf{n}, \tau_0)}$) to evaluate the intralayer (interlayer) expansion error. Here, “ ∞ ” indicates that there is no polynomial approximation for the corresponding part. Figure 4.6 shows the relative errors for 6 electron eigenvalues closest to the Fermi energy along L_{BZ} for three models. We observe that the errors decrease exponentially with τ , \mathbf{m} , \mathbf{n} , which is consistent with the convergence analysis. Although the model becomes more accurate with larger parameters, the model complexity is also higher. From the pictures, we can see that there are some “optimal” parameters to balance the trade-off. For example, we can take

$m = 2, n = 1, \tau = 6$ for the simplified TBG and $m = 2, n = 1, \tau = 2$ for the Wannierized TBG, to achieve the desired accuracy without introducing too much complexity.

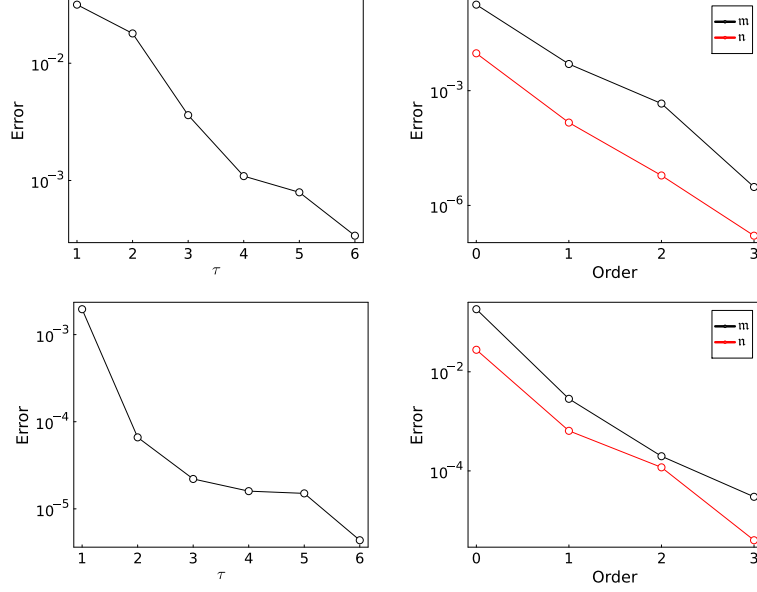


FIGURE 4.6. Relative errors for the 6 electron eigenvalues closest to the Fermi energy along L_{BZ} . The upper pictures show the errors of the simplified TBG, where the first one is for the convergence in hopping truncation τ , and the second one is for the convergence in expansion orders m, n with $\tau_0 = 6$. Similarly for the lower pictures, but for the Wannierized TBG, and $\tau_0 = 2$ for the second one.

We further show the electronic band structures along L_{BZ} for the momentum space model \hat{H} , the BM model $\hat{H}^{(1,0,1)}$, and the high accuracy model $\hat{H}^{(m,n,\tau)}$ (with parameters chosen as above) respectively in Figure 4.7. For the simplified TBG, the momentum space model gives an extremely flat band very close to 0 energy. The BM model gives a slightly less flat band with qualitatively different bands from the momentum space model at the Γ point. This indicates that the BM model of the simplified TBG can not accurately capture these characteristics at the magic angle. By increasing both the intralayer and interlayer expansion orders by one and the hopping truncation parameter by two, the band structure is almost identical to the exact result. Therefore, the parameter choices for the high accuracy continuum model are reasonable. For the Wannierized TBG, the band structure of the BM model is more identical to the exact result except for a slight shift towards 0. This explains why we can use smaller corrections to obtain the accurate mode for the Wannierized TBG compared to the simplified TBG.

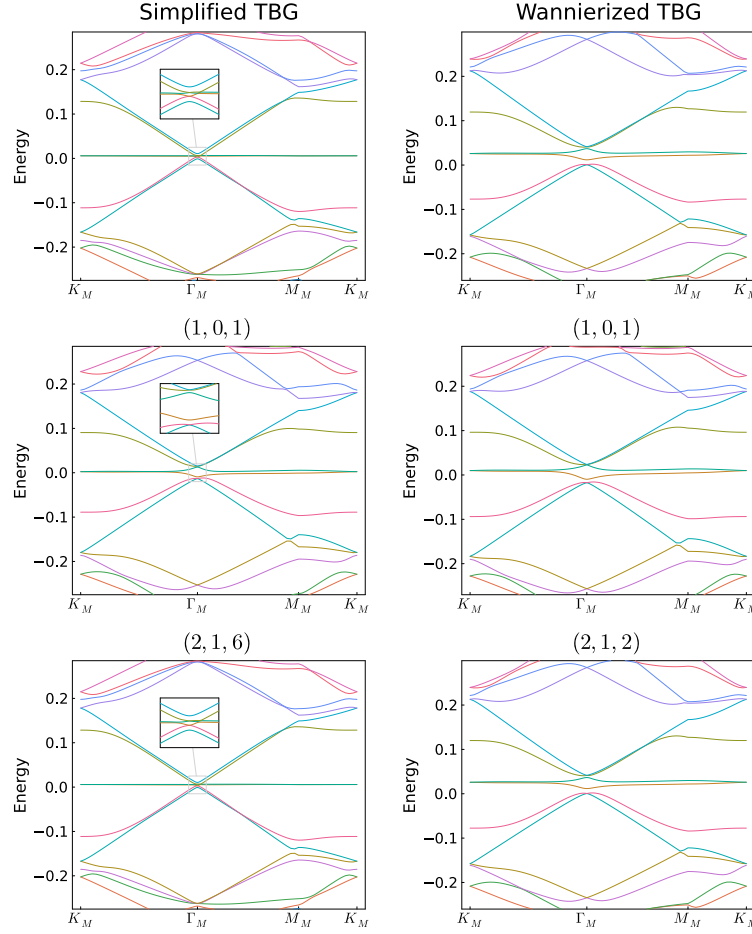


FIGURE 4.7. Magic angle 1.1° electronic band structure along L_{BZ} for three models, the momentum space model (top), the BM model (middle), and the high accuracy continuum model (bottom). The first column shows the band structures for the simplified TBG, while the second shows that of the Wannierized TBG. The momentum axes are labeled in terms of the high-symmetry points of the reciprocal lattice of the moiré supercell, not the monolayer cells.

APPENDIX A. PROOF OF LEMMA 3.1

Since the Taylor series of the hoppings are

$$\tilde{h}_{\sigma\sigma'}^{jj}(\xi) = \sum_{|\beta|=0}^{\infty} \frac{D^\beta \tilde{h}_{\sigma\sigma'}^{jj}(\xi_0)}{\beta!} (\xi - \xi_0)^\beta$$

$$= \sum_{|\beta|=0}^{\infty} \frac{(\xi - \xi_0)^\beta}{\beta!} \sum_{R_j \in \mathcal{R}_j} (-i(\tau_\sigma - \tau_{\sigma'} + R_j))^\beta e^{-i\xi_0 \cdot (\tau_\sigma - \tau_{\sigma'} + R_j)} h_{\sigma\sigma'}^{jj}(R_j),$$

and

$$\begin{aligned} \hat{h}_{\sigma\sigma'}^{12}(\xi) &= \sum_{|\beta|=0}^{\infty} \frac{D^\beta \hat{h}_{\sigma\sigma'}^{12}(\xi_0)}{\beta!} (\xi - \xi_0)^\beta \\ &= \sum_{|\beta|=0}^{\infty} \frac{(\xi - \xi_0)^\beta}{\beta!} \int_{\mathbb{R}^2} (-ix)^\beta e^{-ix \cdot \xi_0} h_{\sigma\sigma'}^{12}(x) dx. \end{aligned}$$

By Assumption 2, 3 and the Cauchy–Schwarz inequality, we have

$$\begin{aligned} |\tilde{h}_{\sigma\sigma'}^{jj}(\xi)| &\leq \sum_{R_j \in \mathcal{R}_j} |h_{\sigma\sigma'}^{jj}(R_j)| \sum_{|\beta|=0}^{\infty} \frac{|(\xi - \xi_0)^\beta (\tau_\sigma - \tau_{\sigma'} + R_j)^\beta|}{\beta!} \\ &\lesssim \sum_{R_j \in \mathcal{R}_j} e^{(|\xi - \xi_0| - \gamma_j)|R_j|}, \end{aligned}$$

and

$$\begin{aligned} |\hat{h}_{\sigma\sigma'}^{12}(\xi)| &\leq \int_{\mathbb{R}^2} \sum_{|\beta|=0}^{\infty} \frac{|(\xi - \xi_0)^\beta x^\beta|}{\beta!} |h_{\sigma\sigma'}^{12}(x)| dx \\ &\lesssim \int_{\mathbb{R}^2} e^{(|\xi - \xi_0| - \gamma_{12})|x|} dx. \end{aligned}$$

We can therefore obtain that the Taylor series converge absolutely for

$$\{q \in \mathbb{R}^2, G \in \mathcal{R}_2^* : |q - \tilde{K}_1 + \mathfrak{G}_M(G)| < \min\{\gamma_1, \gamma_{12}\}\}$$

and

$$\{q \in \mathbb{R}^2, G \in \mathcal{R}_1^* : |q - \tilde{K}_2 + \mathfrak{G}_M(G)| < \gamma_2\}.$$

Similarly, by the Taylor's theorem, we have the following estimates for the remainders,

$$\begin{aligned} &\sum_{|\beta|=m+1} \frac{1}{\beta!} \max_{\xi'} |D^\beta \tilde{h}_{\sigma\sigma'}^{jj}(\xi') (\xi - \xi_0)^\beta| \\ &\lesssim \sum_{k=m+1}^{\infty} \frac{|\xi - \xi_0|^k}{k!} \sum_{R_j \in \mathcal{R}_j} e^{-\gamma_j |R_j|} |\tau_\sigma - \tau_{\sigma'} + R_j|^k \\ &\leq \frac{1}{|\Gamma_j|} \sum_{k=m+1}^{\infty} \frac{|\xi - \xi_0|^k}{k!} \int_{\mathbb{R}^2} |\tau_\sigma - \tau_{\sigma'} + x|^k e^{-\gamma_j |x|} dx \\ &\leq \frac{e^{\gamma_j |\tau_\sigma - \tau_{\sigma'}|}}{|\Gamma_j|} \sum_{k=m+1}^{\infty} \frac{|\xi - \xi_0|^k}{k!} \int_0^{2\pi} \int_0^\infty r^{k+1} e^{-\gamma_j r} dr d\theta \end{aligned}$$

$$\begin{aligned}
&= \frac{2\pi e^{\gamma_j |\tau_\sigma - \tau_{\sigma'}|}}{\gamma_j |\Gamma_j|} \sum_{k=\mathfrak{m}+1}^{\infty} (k+1) \left(\frac{|\xi - \xi_0|}{\gamma_j} \right)^k \\
&\lesssim (\mathfrak{m}+1) \left(\frac{|\xi - \xi_0|}{\gamma_j} \right)^{\mathfrak{m}+1},
\end{aligned}$$

and

$$\begin{aligned}
&\sum_{|\beta|=\mathfrak{n}+1}^{\infty} \frac{1}{\beta!} \max_{\xi'} |D^\beta \hat{h}_{\sigma\sigma'}^{12}(\xi')(\xi - \xi_0)^\beta| \\
&\lesssim \sum_{k=\mathfrak{n}+1}^{\infty} \frac{|\xi - \xi_0|^k}{k!} \int_{\mathbb{R}^2} |x|^k e^{-\gamma_{12}|x|} dx \\
&= \sum_{k=\mathfrak{n}+1}^{\infty} \frac{|\xi - \xi_0|^k}{k!} \int_0^{2\pi} \int_0^\infty r^{k+1} e^{-\gamma_{12}r} dr d\theta \\
&= \frac{2\pi}{\gamma_{12}} \sum_{k=\mathfrak{n}+1}^{\infty} (k+1) \left(\frac{|\xi - \xi_0|}{\gamma_{12}} \right)^k \\
&\lesssim (\mathfrak{n}+1) \left(\frac{|\xi - \xi_0|}{\gamma_{12}} \right)^{\mathfrak{n}+1}.
\end{aligned}$$

Let $\Delta H := \hat{H}_r^{(\tau)}(q) - \hat{H}_r^{(\mathfrak{m}, \mathfrak{n}, \tau)}(q)$, for q, G belonging to the above subsets, we can obtain

$$\begin{aligned}
|(\Delta H_{jj})_{G\sigma, G\sigma'}| &\leq C(\mathfrak{m}+1)(\gamma_j^{-1})^{\mathfrak{m}+1} |q - \tilde{K}_j + \mathfrak{G}_M(G)|^{\mathfrak{m}+1}, \\
|(\Delta H_{12})_{G\sigma, G'\sigma'}| &\leq C(\mathfrak{n}+1)(\gamma_{12}^{-1})^{\mathfrak{n}+1} |q - \tilde{K}_1 + \mathfrak{G}_M(G)|^{\mathfrak{n}+1},
\end{aligned}$$

where the constant C is independent of $\mathfrak{m}, \mathfrak{n}, \tau$.

Note that when $q \in \tilde{K} + \Gamma_M^*$ and $G\sigma \in \Omega_r^*(q)$, we have $|q - \tilde{K}_j + \mathfrak{G}_M(G)| \leq r_\Sigma + r =: r'$. Then we view the matrix as blocks with respect to reciprocal lattices, we can have

$$|(\Delta H_{jj})_{G,G}| \leq C(\mathfrak{m}+1)(\gamma_j^{-1}r')^{\mathfrak{m}+1} \quad \text{and} \quad |(\Delta H_{12})_{G,G'}| \leq C(\mathfrak{n}+1)(\gamma_{12}^{-1}r')^{\mathfrak{n}+1}.$$

Let R_G be the sum of the absolute values of the non-diagonal entries in the G -th row,

$$R_G := \sum_{G' \neq G} |\Delta H_{G,G'}| \leq \sum_{G'} |(\Delta H_{12})_{G,G'}| \delta_{\mathcal{I}(G) + \mathcal{I}(G') \in \mathcal{B}_\tau} \leq C \# \mathcal{B}_\tau (\mathfrak{n}+1) (\gamma_{12}^{-1}r')^{\mathfrak{n}+1}.$$

By the Gershgorin circle theorem, we can obtain

$$\|\Delta H\|_{\text{op}} \leq \max_G (|\Delta H_{G,G}| + R_G) \leq C \left((\mathfrak{m}+1) (\max_{j=1,2} \gamma_j^{-1}r')^{\mathfrak{m}+1} + \# \mathcal{B}_\tau (\mathfrak{n}+1) (\gamma_{12}^{-1}r')^{\mathfrak{n}+1} \right).$$

APPENDIX B. PROOF OF LEMMA 3.2

By the definition of $\tilde{\mathcal{E}}_{q,j}$, and the matrix elements (3.29) and (3.30), for $G_M \sigma \in \Omega_{1M}^*$, we have

$$\begin{aligned}
[\tilde{H}^{(m,n,\tau)}(q)\tilde{\mathcal{E}}_q\tilde{\psi}]_{G_M\sigma}^1 &= \sum_{G'_M\sigma' \in \Omega_{1M}^*} [\tilde{H}_{11}^{(m)}(q)]_{G_M\sigma, G'_M\sigma'} e^{-i\mathfrak{G}_1(G'_M)\cdot\tau_{\sigma'}} \tilde{\psi}_{1\sigma'}(q - \tilde{K}_1 + G'_M) \\
&\quad + \sum_{G'_M\sigma' \in \Omega_{2M}^*} [\tilde{H}_{12}^{(n,\tau)}(q)]_{G_M\sigma, G'_M\sigma'} e^{-i\mathfrak{G}_2(G'_M)\cdot\tau_{\sigma'}} \tilde{\psi}_{2\sigma'}(q - \tilde{K}_2 - G'_M) \\
&= e^{-i\mathfrak{G}_1(G_M)\cdot\tau_\sigma} \sum_{\sigma' \in \mathcal{A}_1} \tilde{P}_{1,\sigma\sigma'}^m(q - \tilde{K}_1 + G_M) \tilde{\psi}_{1\sigma'}(q - \tilde{K}_1 + G_M) \\
&\quad + e^{-i\mathfrak{G}_1(G_M)\cdot\tau_\sigma} \sum_{\sigma' \in \mathcal{A}_2, \mathcal{I}(\tilde{G}_M) \in \mathcal{B}_\tau} e^{i\mathfrak{G}_1(\tilde{G}_M)\cdot\tau_\sigma} e^{-i\mathfrak{G}_2(\tilde{G}_M)\cdot\tau_{\sigma'}} \\
&\quad \tilde{U}_{\mathfrak{G}_1(\tilde{G}_M), \sigma\sigma'}^n(q - \tilde{K}_1 + G_M) \tilde{\psi}_{2\sigma'}(q - \tilde{K}_1 + G_M + \tilde{K}_1 - \tilde{K}_2 - \tilde{G}_M) \\
&= \tilde{\mathcal{E}}_{q,1} \left\{ \sum_{\sigma' \in \mathcal{A}_1} \tilde{P}_{1,\sigma\sigma'}^m(\cdot) \tilde{\psi}_{1\sigma'} + \sum_{\sigma' \in \mathcal{A}_2, \mathcal{I}(\tilde{G}_M) \in \mathcal{B}_\tau} e^{i\mathfrak{G}_1(\tilde{G}_M)\cdot\tau_\sigma} e^{-i\mathfrak{G}_2(\tilde{G}_M)\cdot\tau_{\sigma'}} \right. \\
&\quad \left. \tilde{U}_{\mathfrak{G}_1(\tilde{G}_M), \sigma\sigma'}^n(\cdot) \tilde{\psi}_{2\sigma'}(\cdot + \tilde{K}_1 - \tilde{K}_2 - \tilde{G}_M) \right\}_{G_M\sigma}.
\end{aligned}$$

Therefore, we can deduce that

$$\begin{aligned}
[H_{jj}^{(m)}(q)]_{\sigma\sigma'} &= \tilde{P}_{j,\sigma\sigma'}^m(q), \\
[H_{12}^{(n,\tau)}(q)]_{\sigma\sigma'} &= \sum_{\mathcal{I}(G_M) \in \mathcal{B}_\tau} e^{i\mathfrak{G}_1(G_M)\cdot\tau_\sigma} e^{-i\mathfrak{G}_2(G_M)\cdot\tau_{\sigma'}} \tilde{U}_{\mathfrak{G}_1(G_M), \sigma\sigma'}^n(q) T_{\tilde{K}_1 - \tilde{K}_2 - G_M}.
\end{aligned}$$

APPENDIX C. PROOF OF THEOREM 3.1

We denote the approximate DoS of $\hat{H}_r^{(m,n,\tau)}$ by $D_{\varepsilon,r}^{(m,n,\tau)}(E; \tilde{K})$, and then divide the error into three parts:

$$\begin{aligned}
\left| D_\varepsilon(E) - \sum_{\tilde{K} \in \{K, K'\}} D_\varepsilon^{(m,n,\tau)}(E; \tilde{K}) \right| &\leq \left| D_\varepsilon(E) - \sum_{\tilde{K} \in \{K, K'\}} D_{\varepsilon,r}^{(\tau)}(E; \tilde{K}) \right| \\
&\quad + \sum_{\tilde{K} \in \{K, K'\}} \left| D_{\varepsilon,r}^{(\tau)}(E; \tilde{K}) - D_{\varepsilon,r}^{(m,n,\tau)}(E; \tilde{K}) \right| \\
&\quad + \sum_{\tilde{K} \in \{K, K'\}} \left| D_{\varepsilon,r}^{(m,n,\tau)}(E; \tilde{K}) - D_\varepsilon^{(m,n,\tau)}(E; \tilde{K}) \right| \\
&=: I_1 + I_2 + I_3.
\end{aligned}$$

Since the truncation part I_1 has been given by Theorem 2.2, we only need to quantify polynomial approximation error I_2 and extension error I_3 . For simplicity, we define the following notations to distinguish the intralayer part and interlayer part for a sheet-wise

decomposed matrix $A = \begin{pmatrix} A_{11} & A_{12} \\ A_{12}^\dagger & A_{22} \end{pmatrix}$,

$$A_{\text{intra}} := \begin{pmatrix} A_{11} & 0 \\ 0 & A_{22} \end{pmatrix}, \quad A_{\text{inter}} := \begin{pmatrix} 0 & A_{12} \\ A_{12}^\dagger & 0 \end{pmatrix}.$$

For the polynomial approximation error, we have

$$\begin{aligned} I_2 &\leq \nu^* \int_{\tilde{K} + \Gamma_M^*} |\text{Tr } \delta_\varepsilon(E - \hat{H}_r^{(\tau)}(q)) - \text{Tr } \delta_\varepsilon(E - \hat{H}_r^{(\mathbf{m}, \mathbf{n}, \tau)}(q))| dq \\ &\leq \nu^* \sum_{i=1}^{\#\Omega_r^*(q)} \int_{\tilde{K} + \Gamma_M^*} |\delta_\varepsilon(E - \epsilon_i(q)) - \delta_\varepsilon(E - \epsilon_i(q, \mathbf{m}, \mathbf{n}))| dq, \end{aligned}$$

where $\epsilon_i(q)$ and $\epsilon_i(q, \mathbf{m}, \mathbf{n})$ denote the i -th eigenvalues of $\hat{H}_r^{(\tau)}(q)$ and $\hat{H}_r^{(\mathbf{m}, \mathbf{n}, \tau)}(q)$ respectively, and sorted in ascending order. Let V be the i -dimensional subspace of $\ell^\infty(\Omega_r^*(q))$. For any $\Psi \in V$, $\|\Psi\|_2 = 1$, we have

$$|(\Psi, \hat{H}_r^{(\tau)}\Psi) - (\Psi, \hat{H}_r^{(\mathbf{m}, \mathbf{n}, \tau)}\Psi)| \leq \|\Delta H\|_{\text{op}},$$

where $\Delta H := \hat{H}_r^{(\tau)} - \hat{H}_r^{(\mathbf{m}, \mathbf{n}, \tau)}$. Hence

$$(\Psi, \hat{H}_r^{(\mathbf{m}, \mathbf{n}, \tau)}\Psi) - \|\Delta H\|_{\text{op}} \leq (\Psi, \hat{H}_r^{(\tau)}\Psi) \leq (\Psi, \hat{H}_r^{(\mathbf{m}, \mathbf{n}, \tau)}\Psi) + \|\Delta H\|_{\text{op}}.$$

By the min-max theorem, we obtain that for any $i \in \{1, \dots, \#\Omega_r^*(q)\}$,

$$|\epsilon_i(q) - \epsilon_i(q, \mathbf{m}, \mathbf{n})| \leq \|\Delta H\|_{\text{op}}.$$

We thus have

$$|\delta_\varepsilon(E - \epsilon_i(q)) - \delta_\varepsilon(E - \epsilon_i(q, \mathbf{m}, \mathbf{n}))| \leq \max_x |\delta'_\varepsilon(x)| |\epsilon_i(q) - \epsilon_i(q, \mathbf{m}, \mathbf{n})| \lesssim \varepsilon^{-2} \|\Delta H\|_{\text{op}}.$$

In addition, we note that some error is also controlled by the Gaussian tail. Let $\lambda_i(q)$ be the i -th eigenvalue of $\hat{H}_{r, \text{intra}}^{(\tau)}$, we similarly have

$$|\lambda_i(q) - \epsilon_i(q)| \leq \|\hat{H}_r^{(\tau)} - \hat{H}_{r, \text{intra}}^{(\tau)}\|_{\text{op}} < \frac{\eta}{2},$$

where η is defined in (2.15). Moreover, we separate the eigenvalues by energy windows. Consider an increasing collection of energy $E_k = \Sigma + \frac{k+2}{2}\eta$, $k = -1, \dots, n+1$, satisfying $E_{n-1} < \|\hat{H}_{r, \text{intra}}^{(\tau)}\|_{\text{op}} \leq E_n$. Then for $\lambda_i(q) \in B_{E_k} \setminus B_{E_{k-1}}$, $1 \leq k \leq n$, we have $\epsilon_i(q) \in B_{E_{k+1}} \setminus B_{E_{k-2}}$. Therefore, for i such that $\lambda_i(q) \in B_{E_k} \setminus B_{E_{k-1}}$, there is a constant γ_g such that

$$(3.39) \quad |\delta_\varepsilon(E - \epsilon_i(q))| \lesssim \varepsilon^{-1} e^{-\gamma_g k^2 \varepsilon^{-2}}.$$

And by the conical structure of the monolayer band structure, we have

$$(3.40) \quad \#\{i : \lambda_i(q) \in B_{E_k} \setminus B_{E_{k-1}}\} \sim k.$$

Then by (3.39) and (3.40), we obtain

$$\begin{aligned} \sum_{i, \lambda_i(q) \notin B_{\Sigma+\eta}} |\delta_\varepsilon(E - \epsilon_i(q))| &= \sum_{k=1}^n \sum_{i, \lambda_i(q) \in B_{E_k} \setminus B_{E_{k-1}}} |\delta_\varepsilon(E - \epsilon_i(q))| \\ &\lesssim \varepsilon^{-1} \sum_{k=1}^n k e^{-\gamma_g k^2 \varepsilon^{-2}} \\ &\lesssim \varepsilon^{-1} \int_1^n k e^{-\gamma_g k^2 \varepsilon^{-2}} dk \\ &\lesssim \varepsilon e^{-\gamma_g \varepsilon^{-2}}. \end{aligned}$$

We also note that

$$\#\{i : \lambda_i(q) \in B_{\Sigma+\eta}\} \sim \#\Omega_0^*(\tilde{K}).$$

The analysis is similar for $\epsilon_i(q, \mathbf{m}, \mathbf{n})$. Then by Lemma 3.1, we obtain

$$I_2 \lesssim \varepsilon^{-2} \max_{\tilde{K} \in \{K, K'\}} \#\Omega_0^*(\tilde{K}) \left((\mathbf{m}+1) \left(\max_{j=1,2} \gamma_j^{-1}(r_\Sigma+r) \right)^{\mathbf{m}+1} + \#\mathcal{B}_\tau(\mathbf{n}+1) \left(\gamma_{12}^{-1}(r_\Sigma+r) \right)^{\mathbf{n}+1} \right) + \varepsilon e^{-\gamma_g \varepsilon^{-2}}.$$

We now estimate I_3 . Since $\hat{H}_r^{(\mathbf{m}, \mathbf{n}, \tau)}$ and $\tilde{H}^{(\mathbf{m}, \mathbf{n}, \tau)}$ have same hopping truncation and expansion orders, we could view \mathbf{m}, \mathbf{n} and τ as fixed parameters. For simplicity of notations, we denote for matrices $B(q)$

$$T(B) = \nu^* \int_{\tilde{K} + \Gamma_M^*} B(q) dq,$$

so in particular,

$$D_\varepsilon^{(\mathbf{m}, \mathbf{n}, \tau)}(E; \tilde{K}) = \text{Tr } T(\delta_\varepsilon(E - \tilde{H}^{(\mathbf{m}, \mathbf{n}, \tau)})).$$

Let \mathcal{C} be a contour around the spectrum $\tilde{H}^{(\mathbf{m}, \mathbf{n}, \tau)}$ such that $d(\mathcal{C}, \tilde{H}^{(\mathbf{m}, \mathbf{n}, \tau)}) \in (\varepsilon, 2\varepsilon)$. If the spectrum has gaps larger than ε , then \mathcal{C} would not be a simple curve in the complex plane but a union of one per ungapped interval of spectrum. We observe that

$$I_3 = \frac{1}{2\pi} \left| \oint_{\mathcal{C}} \delta_\varepsilon(E - z) \left(\text{Tr } T((z - \tilde{H}^{(\mathbf{m}, \mathbf{n}, \tau)})^{-1}) - \text{Tr } T((z - \hat{H}_r^{(\mathbf{m}, \mathbf{n}, \tau)})^{-1}) \right) dz \right|.$$

We use the ring decomposition technique from [23] to find the bound of I_3 . We define a new energy range

$$\tilde{\Sigma} := \Sigma + \|\hat{H}_{r, \text{intra}}^{(\mathbf{m}, \mathbf{n}, \tau)} - \hat{H}_{r, \text{intra}}^{(\tau)}\|_{\text{op}},$$

a new enlarge strength

$$\tilde{\eta} := (2 + \alpha) \|\tilde{H}_{\text{inter}}^{(\mathbf{m}, \mathbf{n}, \tau)}\|_{\text{op}}.$$

and a new radius \tilde{r} satisfying $\Gamma_j^*(B_{\tilde{\Sigma}+\tilde{\eta}}) + B_{\tilde{r}}(0) \subseteq \Gamma_j^*(B_{\Sigma+\eta}) + B_r(0)$ and $\Gamma_j^*(B_{\tilde{\Sigma}+\tilde{\eta}}) + B_{\tilde{r}+\delta}(0) \not\subseteq \Gamma_j^*(B_{\Sigma+\eta}) + B_r(0)$ for any $\delta > 0$. Note that $\tilde{r} \approx r$ for \mathbf{m}, \mathbf{n} large enough. Consider an increasing collection of radii $r_0, \dots, r_n, r_{n+1}, r_{n+2} \dots$ such that $r_0 = 0$ and

$r_n = \tilde{r}$. For $q \in \tilde{K} + \Gamma_M^*$, we write $H := \tilde{H}^{(m,n,\tau)}(q)$, and use (2.16), (2.18) to define the following decomposition:

$$\begin{aligned} U_0 &= I(\Omega_{r_0}^*(q, B_{\tilde{\Sigma}+\tilde{\eta}})), \\ U_j &= I(\Omega_{r_j}^*(q, B_{\tilde{\Sigma}+\tilde{\eta}})) \setminus I(\Omega_{r_{j-1}}^*(q, B_{\tilde{\Sigma}+\tilde{\eta}})), \quad j > 0, \\ J_j &= J_{\Omega^* \leftarrow U_j}, \\ H_{ij} &= J_i^* H J_j. \end{aligned}$$

We choose n and $r_j = j\tilde{r}/n$ such that $H_{ij} = 0$ if $|i - j| > 1$, then the decomposition gives a “nearest neighbor” decomposition. Since the sites are coupled in such a way that $\mathcal{I}(G) + \mathcal{I}(G') \in \mathcal{B}_\tau$ or $\mathcal{I}(G_M + G'_M) \in \mathcal{B}_\tau$, this can be easily achieved by choosing n such that the index distance between the sites of two neighboring rings is proportional to

$$C_\tau := \max_{\mathbf{n} \in \mathcal{B}_\tau} |\mathbf{n}|.$$

So we have the number of entries of each ring

$$(3.41) \quad \#U_0 \sim \#\Omega_0^*(\tilde{K}), \quad \#U_j \sim jC_\tau^2, \quad j > 0.$$

We observe that the Hamiltonian is

$$H = \begin{pmatrix} H_{00} & H_{01} & 0 & 0 & \cdots \\ H_{10} & H_{11} & H_{12} & 0 & \cdots \\ 0 & H_{21} & H_{22} & H_{23} & \cdots \\ 0 & 0 & H_{32} & H_{33} & \cdots \\ \vdots & \ddots & \ddots & \ddots & \ddots \end{pmatrix}.$$

We let $H_{i \leftrightarrow j}$ be the matrix restricted to the rings i through j for $i < j$, and $J_{i \leftrightarrow j}$ be the corresponding inclusion. We also use the resolvent notations:

$$R_{i \leftrightarrow j} = (z - H_{i \leftrightarrow j})^{-1}, \quad R_j = (z - H_{jj})^{-1}, \quad R = (z - H)^{-1}.$$

Then by (3.41),

$$\begin{aligned} (3.42) \quad I_3 &\leq \frac{1}{2\pi} \sum_{k=0}^{\infty} \left\| \oint_{\mathcal{C}} \delta_\varepsilon(E - z) (\text{Tr } T(J_k^* R J_k) - \text{Tr } T(J_k^* R_{0 \leftrightarrow n} J_k)) dz \right\| \\ &\lesssim \#\Omega_0^*(\tilde{K}) \left\| \oint_{\mathcal{C}} \delta_\varepsilon(E - z) (T(J_0^* R J_0) - T(J_0^* R_{0 \leftrightarrow n} J_0)) dz \right\|_{\text{op}} \\ &\quad + C_\tau^2 \sum_{k=1}^{\infty} k \left\| \oint_{\mathcal{C}} \delta_\varepsilon(E - z) (T(J_k^* R J_k) - T(J_k^* R_{0 \leftrightarrow n} J_k)) dz \right\|_{\text{op}}. \end{aligned}$$

It suffices to show that for $\forall q \in \tilde{K} + \Gamma_M^*$,

$$(3.43) \quad \left\| \oint_{\mathcal{C}} \delta_\varepsilon(E - z) (J_0^* R J_0 - J_0^* R_{0 \leftrightarrow n} J_0) dz \right\|_{\text{op}} \lesssim \varepsilon^{-4} e^{-\gamma_m r} + \varepsilon^{-1} e^{-\gamma_g \varepsilon^{-2}},$$

$$(3.44) \quad \sum_{k=1}^{\infty} k \left\| \oint_{\mathcal{C}} \delta_{\varepsilon}(E - z) (J_k^* R J_k - J_k^* R_{0 \leftrightarrow n} J_k) dz \right\|_{\text{op}} \lesssim \varepsilon^{-4} (r+1) e^{-\gamma_m r} + \varepsilon e^{-\gamma_g \varepsilon^{-2}}.$$

In the following, we will omit the notation q , and consider two cases for $k \in \{0, \dots, \infty\}$.

Case 1, $k \leq n/2$: We divide \mathcal{C} into two regions,

$$(3.45) \quad \mathcal{C}_k^+ = \left\{ z \in \mathcal{C} : \text{Re}(z) \in B_{\Sigma_k + \tilde{\eta}'} \right\}, \quad \mathcal{C}_k^- \in \mathcal{C} \setminus \mathcal{C}_k^+,$$

where

$$\Sigma_k := \Sigma + \|J_{0 \leftrightarrow k}^* \tilde{H}_{\text{intra}}^{(m,n,\tau)} J_{0 \leftrightarrow k}\|_{\text{op}} - \|J_0^* \tilde{H}_{\text{intra}}^{(m,n,\tau)} J_0\|_{\text{op}}, \quad \tilde{\eta}' := \frac{\alpha}{2} \|\tilde{H}_{\text{inter}}^{(m,n,\tau)}\|_{\text{op}}.$$

We have

$$\begin{aligned} & \oint_{\mathcal{C}} \delta_{\varepsilon}(E - z) (J_k^* R J_k - J_k^* R_{0 \leftrightarrow n} J_k) dz \\ &= \oint_{\mathcal{C}_k^+} \delta_{\varepsilon}(E - z) (J_k^* R J_k - J_k^* R_{0 \leftrightarrow n} J_k) dz + \oint_{\mathcal{C}_k^-} \delta_{\varepsilon}(E - z) (J_k^* R J_k - J_k^* R_{0 \leftrightarrow n} J_k) dz. \end{aligned}$$

We observe that for $z \in \mathcal{C}_k^-$, there is a $\gamma_g > 0$ such that

$$|E - z| \geq \sqrt{2\gamma_g}(k+1),$$

so the second term is bounded by

$$\begin{aligned} & \left\| \oint_{\mathcal{C}_k^-} \delta_{\varepsilon}(E - z) (J_k^* R J_k - J_k^* R_{0 \leftrightarrow n} J_k) dz \right\|_{\text{op}} \lesssim \varepsilon^{-1} \oint_{\mathcal{C}_k^-} |\delta_{\varepsilon}(E - z)| |dz| \\ & \lesssim \varepsilon^{-2} \int_{|E-t| \geq \sqrt{2\gamma_g}(k+1)} e^{-|E-t|^2/2\varepsilon^2} dt \\ & \lesssim \varepsilon^{-1} e^{-\gamma_g(k+1)^2\varepsilon^{-2}}. \end{aligned} \quad (3.46)$$

Hence, it suffices to prove for arbitrary $z \in \mathcal{C}_k^+$, there is a $\lambda > 0$,

$$(3.47) \quad \|J_k^* R J_k - J_k^* R_{0 \leftrightarrow n} J_k\|_{\text{op}} \lesssim \varepsilon^{-3} e^{-\lambda(n-k)}.$$

Note that we can directly obtain (3.43) by taking $k = 0$ for (3.46) and (3.47), and using $n \sim r$. To obtain (3.47), we use the Schur complement for the ring decomposition

$$\begin{aligned} & \|J_k^* R J_k - J_k^* R_{0 \leftrightarrow n} J_k\|_{\text{op}} \\ &= \|J_k^* R_{0 \leftrightarrow n} J_{0 \leftrightarrow n}^* H J_{n+1 \leftrightarrow \infty} J_{n+1 \leftrightarrow \infty}^* R J_{n+1 \leftrightarrow \infty} J_{n+1 \leftrightarrow \infty}^* H J_{0 \leftrightarrow n} R_{0 \leftrightarrow n} J_k\|_{\text{op}} \\ &\lesssim \varepsilon^{-2} \|J_k^* R_{0 \leftrightarrow n} J_n\|_{\text{op}}. \end{aligned}$$

The last inequality is found by noting $J_{0 \leftrightarrow n}^* H J_{n+1 \leftrightarrow \infty} J_{n+1 \leftrightarrow \infty}^*$ only couples ring n on the left to ring $n+1$ on the right. We then rewrite $J_k^* R_{0 \leftrightarrow n} J_n$ using the top right entry in an iterative fashion as follows:

$$J_k^* R_{0 \leftrightarrow n} J_n = J_k^* R_{0 \leftrightarrow n} J_{n-1} H_{n-1,n} R_n$$

$$\begin{aligned}
&= J_k^* R_{0 \leftrightarrow n} J_{n-2} H_{n-2, n-1} J_{n-1}^* R_{n-1 \leftrightarrow n} J_{n-1} H_{n-1, n} R_n \\
&\vdots \\
(3.48) \quad &= J_k^* R_{0 \leftrightarrow n} J_k \prod_{j=k+1}^n H_{j-1, j} J_j^* R_{j \leftrightarrow n} J_j.
\end{aligned}$$

Recalling the definition of $J_{j \leftrightarrow n}$ and \mathcal{C}_k^+ ,

$$\begin{aligned}
&\|H_{j-1, j} J_j^* R_{j \leftrightarrow n} J_j\|_{\text{op}} \\
&\leq \|H_{j-1, j}\|_{\text{op}} \|(z - H_{j \leftrightarrow n})^{-1}\|_{\text{op}} \\
&\leq \|\tilde{H}_{\text{inter}}^{(\mathbf{m}, \mathbf{n}, \tau)}\|_{\text{op}} \left(\min |\sigma(z - J_{j \leftrightarrow n}^* (\tilde{H}^{(\mathbf{m}, \mathbf{n}, \tau)} - \tilde{H}_{\text{inter}}^{(\mathbf{m}, \mathbf{n}, \tau)}) J_{j \leftrightarrow n})| - \|\tilde{H}_{\text{inter}}^{(\mathbf{m}, \mathbf{n}, \tau)}\|_{\text{op}} \right)^{-1} \\
&\leq \|\tilde{H}_{\text{inter}}^{(\mathbf{m}, \mathbf{n}, \tau)}\|_{\text{op}} \left(\min |\sigma(J_{j \leftrightarrow n}^* \tilde{H}_{\text{intra}}^{(\mathbf{m}, \mathbf{n}, \tau)} J_{j \leftrightarrow n})| - |\text{Re}(z)| - \|\tilde{H}_{\text{inter}}^{(\mathbf{m}, \mathbf{n}, \tau)}\|_{\text{op}} \right)^{-1} \\
(3.49) \quad &\leq \frac{1}{1 + \alpha/2}.
\end{aligned}$$

Then by (3.48) and (3.49), we obtain

$$\|J_k^* R_{0 \leftrightarrow n} J_n\|_{\text{op}} \lesssim \varepsilon^{-1} \left(\frac{1}{1 + \alpha/2} \right)^{n-k} = \varepsilon^{-1} e^{-\lambda(n-k)}$$

for some $\lambda > 0$.

Case 2, $k > n/2$: We observe that

$$(3.50) \quad \oint_{\mathcal{C}} \delta_\varepsilon(E - z) J_k^* R J_k dz = \oint_{\mathcal{C}} \delta_\varepsilon(E - z) J_k^* (R - R_{k/2 \leftrightarrow \infty}) J_k dz + 2\pi i J_k^* \delta_\varepsilon(E - H_{k/2 \leftrightarrow \infty}) J_k,$$

$$(3.51) \quad \oint_{\mathcal{C}} \delta_\varepsilon(E - z) J_k^* R_{0 \leftrightarrow n} J_k dz = \oint_{\mathcal{C}} \delta_\varepsilon(E - z) J_k^* (R_{0 \leftrightarrow n} - R_{k/2 \leftrightarrow n}) J_k dz + 2\pi i J_k^* \delta_\varepsilon(E - H_{k/2 \leftrightarrow n}) J_k.$$

We first prove that the first term of (3.50) is bounded by

$$\left\| \oint_{\mathcal{C}} \delta_\varepsilon(E - z) J_k^* (R - R_{k/2 \leftrightarrow \infty}) J_k dz \right\|_{\text{op}} \lesssim \varepsilon^{-4} e^{-\lambda k/2} + \varepsilon^{-1} e^{-\gamma_g(k+1)^2 \varepsilon^{-2}}.$$

Likewise, we divide \mathcal{C} into \mathcal{C}_k^+ and \mathcal{C}_k^- as (3.45), but with

$$\Sigma_k := \Sigma + \|J_{0 \leftrightarrow k/2-1}^* \tilde{H}_{\text{intra}}^{(\mathbf{m}, \mathbf{n}, \tau)} J_{0 \leftrightarrow k/2-1}\|_{\text{op}} - \|J_0^* \tilde{H}_{\text{intra}}^{(\mathbf{m}, \mathbf{n}, \tau)} J_0\|_{\text{op}}.$$

For the \mathcal{C}_k^- term, we have the same bound as for (3.46). Hence, it suffices to show that for $z \in \mathcal{C}_k^+$,

$$\|J_k^* (R - R_{k/2 \leftrightarrow \infty}) J_k\|_{\text{op}} \lesssim \varepsilon^{-3} e^{-\lambda k/2}.$$

We observe that

$$\begin{aligned}
& \|J_k^*(R - R_{k/2 \leftrightarrow \infty})J_k\|_{\text{op}} \\
&= \|J_k^* R_{k/2 \leftrightarrow \infty} J_{k/2 \leftrightarrow \infty}^* H J_{0 \leftrightarrow k/2-1} J_{0 \leftrightarrow k/2-1}^* R J_{0 \leftrightarrow k/2-1} J_{0 \leftrightarrow k/2-1}^* H J_{k/2 \leftrightarrow \infty} R_{k/2 \leftrightarrow \infty} J_k\|_{\text{op}} \\
&\lesssim \varepsilon^{-2} \|J_k^* R_{k/2 \leftrightarrow \infty} J_{k/2}\|_{\text{op}}.
\end{aligned}$$

We next rewrite $J_k^* R_{k/2 \leftrightarrow \infty} J_{k/2}$ using the bottom left entry in an iterative fashion as follows:

$$\begin{aligned}
& J_k^* R_{k/2 \leftrightarrow \infty} J_{k/2} \\
&= J_k^* R_{k/2+1 \leftrightarrow \infty} J_{k/2+1} H_{k/2+1, k/2} J_{k/2}^* R_{k/2 \leftrightarrow \infty} J_{k/2} \\
&= J_k^* R_{k/2+2 \leftrightarrow \infty} J_{k/2+2} H_{k/2+2, k/2+1} J_{k/2+1}^* R_{k/2+1 \leftrightarrow \infty} J_{k/2+1} H_{k/2+1, k/2} J_{k/2}^* R_{k/2 \leftrightarrow \infty} J_{k/2} \\
&\vdots \\
&= J_k^* R_{k \leftrightarrow \infty} J_k \prod_{j=k/2}^{k-1} H_{j+1, j} J_j^* R_{j \leftrightarrow \infty} J_j.
\end{aligned}$$

By the same argument above

$$\|J_k^* R_{k/2 \leftrightarrow \infty} J_{k/2}\|_{\text{op}} \lesssim \varepsilon^{-1} \left(\frac{1}{1 + \alpha/2} \right)^{k/2} = \varepsilon^{-1} e^{-\lambda k/2}.$$

We next show that

$$\|J_k^* \delta_\varepsilon(E - H_{k/2 \leftrightarrow \infty})J_k\|_{\text{op}} \lesssim \varepsilon^{-1} e^{-\gamma_g(k+1)^2 \varepsilon^{-2}}.$$

We observe

$$\min |\sigma(H_{k/2 \leftrightarrow \infty})| \geq \min |\sigma(J_{k/2 \leftrightarrow \infty}^* \tilde{H}_{\text{intra}}^{(\mathbf{m}, \mathbf{n}, \tau)} J_{k/2 \leftrightarrow \infty})| - \|J_{k/2 \leftrightarrow \infty}^* \tilde{H}_{\text{inter}}^{(\mathbf{m}, \mathbf{n}, \tau)} J_{k/2 \leftrightarrow \infty}\|_{\text{op}}.$$

Here the spectrum of $J_{k/2 \leftrightarrow \infty}^* \tilde{H}_{\text{intra}}^{(\mathbf{m}, \mathbf{n}, \tau)} J_{k/2 \leftrightarrow \infty}$ can be approximated to increase linearly with k . The reason for this is that for large \mathbf{m} , the spectrum of $J_{k/2 \leftrightarrow n}^* \tilde{H}_{\text{intra}}^{(\mathbf{m}, \mathbf{n}, \tau)} J_{k/2 \leftrightarrow n}$ is a conical structure, and $J_{n+1 \leftrightarrow \infty}^* \tilde{H}_{\text{intra}}^{(\mathbf{m}, \mathbf{n}, \tau)} J_{n+1 \leftrightarrow \infty}$ only contains 1 order and negligible higher order modifications. We also have $\|J_{k/2 \leftrightarrow \infty}^* \tilde{H}_{\text{inter}}^{(\mathbf{m}, \mathbf{n}, \tau)} J_{k/2 \leftrightarrow \infty}\|_{\text{op}}$ is bounded, since for large \mathbf{n} , $\|J_{k/2 \leftrightarrow n}^* \tilde{H}_{\text{inter}}^{(\mathbf{m}, \mathbf{n}, \tau)} J_{k/2 \leftrightarrow n}\|_{\text{op}}$ is close to $\|\hat{H}_{\text{inter}}\|_{\text{op}}$, and $J_{n+1 \leftrightarrow \infty}^* \tilde{H}_{\text{inter}}^{(\mathbf{m}, \mathbf{n}, \tau)} J_{n+1 \leftrightarrow \infty}$ only contains 0 order and negligible higher order modifications. We then obtain

$$\min |\sigma(H_{k/2 \leftrightarrow \infty})| \gtrsim k + 1,$$

and hence

$$\|\delta_\varepsilon(E - H_{k/2 \leftrightarrow \infty})\|_{\text{op}} \lesssim \varepsilon^{-1} e^{-\gamma_g(k+1)^2 \varepsilon^{-2}}.$$

Using the same argument above, for $n/2 < k \leq n$, (3.51) is similarly bounded by

$$\left\| \oint_{\mathcal{C}} \delta_\varepsilon(E - z) J_k^* R_{0 \leftrightarrow n} J_k dz \right\|_{\text{op}} \lesssim \varepsilon^{-4} e^{-\lambda k/2} + \varepsilon^{-1} e^{-\gamma_g(k+1)^2 \varepsilon^{-2}}.$$

Therefore, we have

$$\begin{aligned}
& \sum_{k=1}^{\infty} k \left\| \oint_{\mathcal{C}} \delta_{\varepsilon}(E - z) (J_k^* R J_k - J_k^* R_{0 \leftrightarrow n} J_k) dz \right\|_{\text{op}} \\
& \lesssim \sum_{k=1}^{n/2} k \varepsilon^{-4} e^{-\lambda(n-k)} + \sum_{k=n/2+1}^{\infty} k \varepsilon^{-4} e^{-\lambda k/2} + \sum_{k=1}^{\infty} k \varepsilon^{-1} e^{-\gamma_g(k+1)^2 \varepsilon^{-2}} \\
& \lesssim \varepsilon^{-4} \left(\int_1^{n/2} k e^{-\lambda(n-k)} dk + \int_{n/2+1}^{\infty} k e^{-\lambda k/2} dk \right) + \varepsilon^{-1} \int_1^{\infty} k e^{-\gamma_g(k+1)^2 \varepsilon^{-2}} dk \\
& \sim \varepsilon^{-4} (r+1) e^{-\lambda r} + \varepsilon e^{-\gamma_g \varepsilon^{-2}},
\end{aligned}$$

where we use $n \sim r$. Combining (3.42)-(3.44), we obtain

$$I_3 \lesssim (\#\Omega_0^*(\tilde{K}) + C_{\tau}^2(r+1)) \varepsilon^{-4} e^{-\lambda r} + (\#\Omega_0^*(\tilde{K}) + \varepsilon^2 C_{\tau}^2) \varepsilon^{-1} e^{-\gamma_g \varepsilon^{-2}}.$$

REFERENCES

- [1] Harry Bateman. *Tables of integral transforms Volume 2*. McGraw-Hill Book Company, 1954.
- [2] Simon Becker, Mark Embree, Jens Wittsten, and Maciej Zworski. Spectral characterization of magic angles in twisted bilayer graphene. *Physical Review B*, 103, 4 2021.
- [3] Simon Becker, Mark Embree, Jens Wittsten, and Maciej Zworski. Mathematics of magic angles in a model of twisted bilayer graphene. *Probability and Mathematical Physics*, 3:69–103, 2022.
- [4] Simon Becker, Tristan Humbert, and Maciej Zworski. Integrability in the chiral model of magic angles. *arXiv:2208.01620*, 2022.
- [5] Simon Becker, Lin Lin, and Kevin D. Stubbs. Exact ground state of interacting electrons in magic angle graphene. *arXiv:2312.15314*, 2023.
- [6] B. Andrei Bernevig, Biao Lian, Aditya Cowsik, Fang Xie, Nicolas Regnault, and Zhi-Da Song. Twisted bilayer graphene. V. Exact analytic many-body excitations in Coulomb Hamiltonians: Charge gap, Goldstone modes, and absence of Cooper pairing. *Phys. Rev. B*, 103:205415, 2021.
- [7] Rafi Bistritzer and Allan H. MacDonald. Moiré bands in twisted double-layer graphene. *Proceedings of the National Academy of Sciences of the United States of America*, 108:12233–12237, 2011.
- [8] Éric Cancès, Louis Garrigue, and David Gontier. Simple derivation of moiré-scale continuous models for twisted bilayer graphene. *Phys. Rev. B*, 107:155403, 2023.
- [9] Éric Cancès and Long Meng. Semiclassical analysis of two-scale electronic Hamiltonians for twisted bilayer graphene. *arXiv:2311.14011*, 2023.
- [10] Yuan Cao, Valla Fatemi, Ahmet Demir, Shiang Fang, Spencer L. Tomarken, Jason Y. Luo, Javier D. Sanchez-Yamagishi, Kenji Watanabe, Takashi Taniguchi, Efthimios Kaxiras, Ray C. Ashoori, and Pablo Jarillo-Herrero. Correlated insulator behaviour at half-filling in magic-angle graphene superlattices. *Nature*, 556:80–84, 2018.
- [11] Yuan Cao, Valla Fatemi, Shiang Fang, Kenji Watanabe, Takashi Taniguchi, Efthimios Kaxiras, and Pablo Jarillo-Herrero. Unconventional superconductivity in magic-angle graphene superlattices. *Nature*, 556:43–50, 2018.
- [12] S Carr, D Massatt, S B Torrisi, P Cazeaux, M Luskin, and E Kaxiras. Relaxation and domain formation in incommensurate two-dimensional heterostructures. *Phys. Rev. B*, 98:224102, 2018.
- [13] Stephen Carr, Daniel Massatt, Mitchell Luskin, and Efthimios Kaxiras. Duality between atomic configurations and bloch states in twistrionic materials. *Phys. Rev. Research*, 2:33162, 7 2020.

- [14] Paul Cazeaux, Mitchell Luskin, and Daniel Massatt. Energy minimization of two dimensional incommensurate heterostructures. *Archive for Rational Mechanics and Analysis*, 235:1289 – 1325, February 2020.
- [15] Trithep Devakul, Valentin Crépel, Yang Zhang, and Liang Fu. Magic in twisted transition metal dichalcogenide bilayers. *Nature Communications*, 12(1):6730, 2021.
- [16] Shiang Fang, Stephen Carr, Miguel A. Cazalilla, and Efthimios Kaxiras. Electronic structure theory of strained two-dimensional materials with hexagonal symmetry. *Phys. Rev. B*, 98:075106, 2018.
- [17] Shiang Fang and Efthimios Kaxiras. Electronic structure theory of weakly interacting bilayers. *Phys. Rev. B*, 93:235153, 2016.
- [18] Fabian M. Faulstich, Kevin D. Stubbs, Qinyi Zhu, Tomohiro Soejima, Rohit Dilip, Huanchen Zhai, Raehyun Kim, Michael P. Zaletel, Garnet Kin-Lic Chan, and Lin Lin. Interacting models for twisted bilayer graphene: A quantum chemistry approach. *Phys. Rev. B*, 107:235123, Jun 2023.
- [19] Zeyu Hao, A. M. Zimmerman, Patrick Ledwith, Eslam Khalaf, Danial Haie Najafabadi, Kenji Watanabe, Takashi Taniguchi, Ashvin Vishwanath, and Philip Kim. Electric field-tunable superconductivity in alternating-twist magic-angle trilayer graphene. *Science*, 371(6534):1133–1138, 2021.
- [20] Michael Hott, Alexander B. Watson, and Mitchell Luskin. From incommensurate bilayer heterostructures to Allen–Cahn: An exact thermodynamic limit. *Archive for Rational Mechanics and Analysis*, 248(6):103, Oct 2024.
- [21] Michael Hott, Alexander B. Watson, and Mitchell Luskin. Mathematical foundations of phonons in incommensurate materials. *arXiv:2409.06151*, 2024.
- [22] Daniel Massatt, Stephen Carr, and Mitchell Luskin. Efficient computation of kubo conductivity for incommensurate 2d heterostructures. *European Physical Journal B*, 93, 2020.
- [23] Daniel Massatt, Stephen Carr, and Mitchell Luskin. Electronic observables for relaxed bilayer two-dimensional heterostructures in momentum space. *Multiscale Modeling & Simulation*, 21(4):1344–1378, 2023.
- [24] Daniel Massatt, Stephen Carr, Mitchell Luskin, and Christoph Ortner. Incommensurate heterostructures in momentum space. *Multiscale Modeling & Simulation*, 16:429–451, 2018.
- [25] Daniel Massatt, Mitchell Luskin, and Christoph Ortner. Electronic density of states for incommensurate layers. *Multiscale Modeling and Simulation*, 15:476–499, 2017.
- [26] Naoto Nakatsuji, Takuto Kawakami, and Mikito Koshino. Multiscale lattice relaxation in general twisted trilayer graphenes. *Phys. Rev. X*, 13:041007, 2023.
- [27] Solomon Quinn, Tianyu Kong, Mitchell Luskin, and Alexander B. Watson. Higher-order continuum models for twisted bilayer graphene. *arXiv:2502.08120*, 2025.
- [28] Mariya Romanova and Vojtěch Vlček. Stochastic many-body calculations of moiré states in twisted bilayer graphene at high pressures. *npj Computational Materials*, 8(1):11, 2022.
- [29] Kevin D. Stubbs, Simon Becker, and Lin Lin. On the Hartree-Fock ground state manifold in magic angle twisted graphene systems. *arXiv:2403.19890*, 2024.
- [30] Grigory Tarnopolsky, Alex Jura Kruchkov, and Ashvin Vishwanath. Origin of magic angles in twisted bilayer graphene. *Physical Review Letters*, 122, 2019.
- [31] Ting Wang, Hua-jie Chen, Aihui Zhou, Yuzhi Zhou, and Daniel Massatt. Convergence of the planewave approximations for quantum incommensurate systems. *Multiscale Modeling & Simulation*, 23(1):545–576, 2025.
- [32] Alexander B. Watson, Tianyu Kong, Allan H. MacDonald, and Mitchell Luskin. Bistritzer–MacDonald dynamics in twisted bilayer graphene. *Journal of Mathematical Physics*, 64(3):031502, 03 2023.
- [33] Alexander B. Watson and Mitchell Luskin. Existence of the first magic angle for the chiral model of bilayer graphene. *Journal of Mathematical Physics*, 091502, 2021.
- [34] Xi Zhang, Kan-Ting Tsai, Ziyang Zhu, Wei Ren, Yujie Luo, Stephen Carr, Mitchell Luskin, Efthimios Kaxiras, and Ke Wang. Correlated insulating states and transport signature of superconductivity in twisted trilayer graphene superlattices. *Phys. Rev. Lett.*, 127:166802, 2021.

- [35] Éric Cancès, Louis Garrigue, and David Gontier. Second-order homogenization of periodic schrödinger operators with highly oscillating potentials. *arXiv:2112.12008*, 2021.

(Xue Quan) BEIJING NORMAL UNIVERSITY, BEIJING, CHINA

Email address: `xuequan@mail.bnu.edu.cn`

(Alexander B. Watson) UNIVERSITY OF MINNESOTA, MINNEAPOLIS, MINNESOTA, U.S.A.

Email address: `abwatson@umn.edu`

(Daniel Massatt) LOUISIANA STATE UNIVERSITY, BATON ROUGE, LOUISIANA, U.S.A.

Email address: `dmassatt@lsu.edu`